A QM STUDY ON DETERMINATION OF VIBRATIONAL FREQUENCIES OF THE SURFACE COORDINATED SPECIES INVOLVED IN CDRM

by

Burcu Karagöz

B.S., Chemical Engineering, Boğaziçi University, 2012

Submitted to the Institute for Graduate Studies in
Science and Engineering in partial fulfillment of
the requirements for the degree of
Master of Science

Graduate Program in Chemical Engineering

Boğaziçi University

2014

"*Sevgilerde…"*

ACKNOWLEDGEMENTS

Foremost, I would like to express my deepest gratitude to my supervisor Prof. Ahmet Erhan Aksoylu for his patience, help, motivation, and encouragement throughout my thesis. His guidance and valuable advices enlighten me not only in academic level but also in my daily life, for which I am extremely grateful.

I am very grateful to my thesis committee Prof. Ramazan Yıldırım and Assoc. Prof. Kunt Atalık for devoting their valuable time to read and comment on my thesis.

I would like to acknowledge Merve Ayvaz who teaches me how to use Materials Studio and DMol^3 in first place. I would like to offer my special thanks to Ali Uzun for his great contribution during teaching me CASTEP and DFT in detailed. Without his support and guidance this study would have been a lot harder for me.

I would like to express my appreciation to the current and old members of KB405, Bilge Kerem Aksakal, Barış Burnak, Elif Can, Çağla Odabaşı, Selen Solak, İbrahim Şimşek, and honorary member Salih Emre Demirel for their valuable friendship, endless motivation and support.

I would like to thank other members of Prof. Aksoylu's group; Burcu Selen Çağlayan, Melek Selcen Başar, Aysun İpek Paksoy, Belkız Merve Eropak, Elif Erdinç, Serhat Erşahin, Coşar Doğa Demirhan, Hazal Bal, Burcu Acar, and Cansu Yassı. Thanks to our weekly meetings, I gained an intuition to experimental studies. You all made my Wednesdays cheerful and full of science. I would also like to thank other CATREL members and my colleagues; Özgür Yaşar Çağlar, Can Ekici, Çiğdem Ekmen, Didem Büşra Kabakçı, Hayri Onur Kavaklı, Sinan Koç, Aybüke Leba, Manouchehr Nadjafi, Sezin Sezen, Zeynep Erge Akbaş, Begüm Alaybeyoğlu, Utku Deniz, Gökçe Ezeroğlu, Elif Gençtürk, Büşra Gürses, Aslı Karademir, Zeynep Kürkçüoğlu, Serdar Özsezen, and Fidan Sümbül for their friendship, and making this period more endurable in many ways.

My sincere thanks also go to Melike Gürbüz, Başak Ünen, Bilgi Dedeoğlu, Belgin Balkan, Yakup Bal, and Murat Düzgünoğlu for their administrative and technical support.

I wish to express my heartfelt thanks to Özge Ertem who is always there whenever I need her. Sharing the same fear and happiness make us closer, hope our friendship lasts forever. I would also like to thank Melis Yıldırım for being supportive and encouraging during my PhD. applications.

Special thanks to Volkan Cirik for his endless love, caring, and understanding. He was always beside me during the happy and hard moments to help me and motivate me.

Last but not the least I would like to thank my parents Hamiyet and Sami Karagöz, and my sister Melis Karagöz Ruhioğlu for their unconditional love, great patience, and everlasting support spiritually throughout my life.

The financial support provided by Boğaziçi University Research Fund through project BAP M6755, and by TÜBİTAK through project 111M144.

ABSTRACT

A QM STUDY ON DETERMINATION OF VIBRATIONAL FREQUENCIES OF THE SURFACE COORDINATED SPECIES INVOLVED IN CDRM

The determination of the sites participating the reaction mechanism is of crucial importance in catalysis. Ni- and Co- based catalysts have been studied by our group for their activity in Catalytic Dry Reforming of Methane (CDRM). Although in-situ FTIR-DRIFT tests have been conducted on those catalysts under adsorption and reaction conditions, and the vibrational spectra were obtained, the available information in the literature is not detailed and surface specific enough to allow the determination of the active sites on the catalyst. The aim of this study is to obtain a vibrational frequency database for the species involved in CDRM reaction mechanism occurs on the possible active faces of the Co- and Ni- based catalysts. In the formation of the database, quantum mechanical simulations utilizing Density Functional Theory (DFT) calculations are used. In the simulations, the metallic faces whose presences have been confirmed for our CDRM catalysts by XRD were considered. Vibrational frequencies of CH_x(x=0-4), CO_2, CO, O and H on Co(111) flat surface, Ni(220) and NiPt(220) terraced surfaces were calculated for each possible sites via DMol^3 tool of Accelrys Materials Studio. Calculated vibrational frequencies of CO_2, CO, CH_3, and CH_2 on Co(111) are in good agreement with the literature. Adsorption energies of CO_2, CO, O, CH_4, CH_3, and CH_2 on Co(111) are inversely related with their stretching frequencies whereas there is a linear relationship for adsorbed CH, C, and H on Co(111). Furthermore, calculated vibrational frequencies of CO_2, CO and CH_2 on Ni(220) are consistent with the literature, while stretching frequency of CH_3 is far different from experimental findings, due to possible alloy formation, and geometry and/or support effect. Comparative analysis of the results obtained for Ni(220) and NiPt(220) revealed that for NiPt(220) surface, Pt existence affect the vibrational frequencies of all species. Moreover, CO_2 and CO vibrational frequencies on NiPt(220) are considerably close to experimental findings. Vibrational frequency of CH_4 is inconsistent with the literature for all surfaces, most probably because the weak CH_4 adsorption on these surfaces may not be precisely calculated by DFT.

ÖZET

CDRM REAKSİYONUNDA VAROLAN YÜZEY KOORDİNELİ MOLEKÜL VE ATOMLARIN TİTREŞİM FREKANSININ BELİRLENMESİ ÜZERİNE QM ÇALIŞMASI

Reaksiyon mekanizmasında rol alan sitelerin belirlenmesi katalizörler için çok önemlidir. Ni ve Co bazlı katalizörlerin aktivitesi Metanın Kuru Reformlanması (CDRM) reaksiyonunda grubumuzca çalışılmıştır. Bu katalizörler üzerinde adsorbsiyon ve reaksiyon koşullarında FTIR-DRIFT testleri yapılmasına, ve titreşim spektrumu elde edilmesine karşın; literatürdeki mevcut bilgiler, katalizör üzerindeki aktif sitelerin FTIR-DRIFT verileri ile karşılaştırmalı olarak incelenebilmesi için yeterince detaylı ve yüzeye özel değildir. Bu çalışmanın amacı, CDRM reaksiyon mekanizmasında varolan ve Co- ve Ni-bazlı katalizörlerin muhtemel aktif yüzlerinde oluşan atom ve moleküller için titreşim frekansı veritabanı oluşturmaktır. Veritabanı oluşturulurken QM simülasyonları ile DFT hesaplamalarından yararlanılmıştır. Simülasyonlarda, bizim grubun çalıştığı CDRM katalizörlerinin XRD analizi ile belirlenen metalik yüzleri göz önünde bulundurulmuştur. Co(111) düz yüzeyinin, ve Ni(220) ve NiPt(220) teraslı yüzeylerin her muhtemel sitesinde CH_x(x=0-4), CO_2, CO, O ve H'nin titreşim frekansları, DMol^3 Accelerys Materials Studio programı vasıtasıyla hesaplanmıştır. Co(111) üzerinde hesaplanmış CO_2, CO, CH_3, ve CH_2'nin titreşim frekansları literatürle uyumludur. Co(111) koordineli CH_4, CH_3, ve CH_2'nin adsorpsiyon enerjisi ile titreşim frekansları arasında ters bir bağıntı varken, CH, C ve H'nin adsorpsiyon enerjisi ile titreşim frekansları arasında doğru bir orantı vardır. Ni(220) yüzeyinde, CO_2, CO and CH_2'nin hesaplanan titreşim frekansları literatürle uyum sağlamaktayken, CH_3 molekülünün titreşim frekansı deneysel bulgudan çok farklıdır. Bu fark, muhtemel alaşım oluşumundan ve geometri ve/veya support etkisinden kaynaklanabilir ki support katalizörün elektronik yapısını büyük ölçüde değiştirebilir. NiPt(220)yüzeyi Ni(220) yüzeyi ile karşılaştırıldığında, NiPt(220) yüzeyinde Pt varlığı tüm molekül ve atomların titreşim frekansını etkilemiştir. NiPt(220) üzerindeki CO_2 ve CO'nun titreşim frekansı deneysel bulgulara oldukça yakındır. Tüm yüzeylerde CH_4'ün titreşim frekansı litertürle uyumlu değildir, bunun büyük nedeni bu yüzeylerdeki zayıf CH_4 adsorpsiyonun DFT ile kesin olarak hesaplanamamasıdır.

TABLE OF CONTENTS

LIST OF FIGURES

LIST OF TABLES

LIST OF SYMBOLS

E	Total energy
E_J	Coulomb energy
E_T	Kinetic energy
E_V	Electron-nuclear interaction energy
E_{XC}	Exchange/correlation energy
$\hat{H}$	Hamiltonian
r	Distance between the nucleus and the electrons
Z	Nucleus charge
ΔG_{1073}	Gibbs free energy of reaction at 1073 K (kj/mol)
ΔG_{298}	Standard Gibbs free energy of reaction (kj/mol)
ΔH	Enthalpy of the reaction (kj/mol)
ΔH_{298}	Standard enthalpy of the reaction (kj/mol)
ε_{XC}	Exchange correlation energy per particle of homogenous electron gas density
ν	Vibrational frequency (cm^{-1})
ρ	Total electron density
ϕ	Hartree-Fock wave function
χ	One electron orbitals
ψ	Wave function
ψ_i	Wave function of electronic state i
*	Active metal sites

LIST OF ACRONYMS/ABBREVIATIONS

AC	Activated Carbon
AER	All Electron Relativistic
BET	Brunauer–Emmett–Teller
CASTEP	Cambridge Serial Total Energy Package
CDRM	Catalytic Dry Reforming of Methane
CI	Configuration Interaction
DFT	Density Functional Theory
DNP	Double Numeric with Polarization
DRIFT	Diffuse Reflectance Infrared Fourier Transform Spectroscopy
ER	Eley-Rideal
FCC	Face Centered Cubic
FH	Fourfold Hollow
FTIR	Fourier Transform Infrared Spectroscopy
GGA	Generalized-Gradient Approximation
HCP	Hexagonal Closed Packed
LB	Long-Bridge
LDA	Local-Density Approximation
LDOS	Local Density of States
LST/QST	Linear Synchronous Transit/Quadratic Synchronous Transit
MLE	Monolayer Equivalent
MP	Møller-Plesset models
MP2	Second-order Møller-Plesset model
MS	Materials Studio

PAW	Projector Augmented Wave
PBE	Perdew-Burke-Ernzerhof
PILC	Pillared Layered Clays
POX	Partial Oxidation
PW91	Perdew-Wang exchange correlation
PWC	Perdew-Wang
QM	Quantum Mechanicals
RPBE	Revised Perdew-Burke-Ernzerhof
RWGS	Reverse Water Gas Shift
SB	Short-Bridge
SCF	Self-Consistent Field
SR	Steam Reforming
TGA	Thermo Gravimetric Analysis
TOS	Time-On-Stream
TPO	Temperature Programmed Oxidation
TPR	Temperature-Programmed Reduction
VASP	Vienna Ab-initio Simulation Package
XPS	X-Ray Photoelectron Spectroscopy
XRD	X-Ray Diffraction

1. INTRODUCTION

There is an increasing trend in World's energy demand. The common usage of fossil fuels affects environment, and human's health (Fechete *et al.*, 2012). Due to these concerns, the new ways of clean energy production are investigated to reduce the emission of greenhouse gases such as CO_2 and CH_4. Annual CO_2 emission based on human activities predicted as 2×10^{15} g of carbon. There is a relation between the global temperature increase and the amounts of CH_4 and CO_2 emission to the atmosphere (Bradford and Vannice, 1999). Therefore, CH_4 and CO_2 utilization has taken attention of the researchers.

Catalytic Dry Reforming of Methane (CDRM) (Equation 1.1) consumes two main greenhouse gases, CH_4 and CO_2, and produces synthesis gas ($CO+H_2$) with H_2/CO ratio to unity, which is preferable for Fischer-Tropsch synthesis to produce liquid fuel and oxygenated compounds (Zhu *et al*., 2009; Liu *et al*., 2011). As the product of CDRM has H_2/CO ratio as 1, it is more advantageous compared to alternative reforming routes, steam reforming (SR) (Equation 1.2) and partial oxidation (POX) (Equation 1.3) (Özkara-Aydınoğlu and Aksoylu, 2011). While methane-reforming reactions are endothermic and require external heat, partial oxidation reaction is exothermic, but it needs oxygen or air (Lunsford, 2000). CDRM is a desirable reaction in areas where water is unavailable (Bradford and Vannice, 1999). Cost of the reactants (CH_4 & CO_2) of CDRM is very low. Natural gas fields consist of CH_4 mostly, however some fields contain CO_2 in concentrations 5 to 100%. CDRM can be used in these reservoirs to produce valuable products from natural gas with lower cost especially in remote regions (Stagg-Williams *et al*., 2000).

$$CH_4 + CO_2 \leftrightarrow 2CO + 2H_2 \qquad \Delta H^o_{298} = +247 \text{ kj mol}^{-1} \qquad (1.1)$$

$$CH_4 + H_2O \leftrightarrow CO + 3H_2 \qquad \Delta H^o_{298} = +206 \text{ kj mol}^{-1} \qquad (1.2)$$

$$CH_4 + \frac{1}{2}O_2 \leftrightarrow CO + 2H_2 \qquad \Delta H^o_{298} = -38 \text{ kj mol}^{-1} \qquad (1.3)$$

CDRM has high thermodynamic potential (ΔG_{298} = 174.6 kJ mol^{-1}) therefore it needs very high temperatures to achieve high conversion (for example ΔG_{1073} = −44.76 kJ mol^{-1}) (Valderrama *et al*., 2013). These conditions lead to sintering of metallic phase and deactivation of catalysts by carbon formation (Özkara-Aydınoğlu *et al*., 2009). Coke deposition may occur via CH_4 decomposition or CO disproportionation, the former becomes the primary reason of coke formation at high temperatures. (Bradford and Vannice, 1999).

Catalysts for CDRM have been developed for many years. Noble metal, such as Pt, Ru and Rh containing catalysts, present high activity, selectivity and stability. However, high cost and low availability of noble metals make them economically unfeasible (Luisetto *et al.*, 2012; Liu *et al.*, 2013). Although non-noble metal catalysts like Fe, Co and Ni deactivated by coke deposition, they are preferable due to their low cost, high availability and activity (Liu *et al.*, 2013; Yu *et al.*, 2012; San-José-Alonso *et al.*, 2011). Ni and Co catalysts suffer mostly from sintering of metal and formation of carbon on their surfaces. The stability of these catalysts can be enhanced by addition of metals and by using suitable supports. The catalyst can be prevented from coke deposition, by adjusting acid-base and redox characteristics of it via distinct promoters (Yu *et al*., 2012; San-José-Alonso *et al.*, 2011). These metals supported on oxide systems such as MgO–ZrO_2, Al_2O_3, $MgAl_2O_4$, CeO_2, CeO_2–ZrO_2 and they exhibit promising performances (Luisetto *et al.*, 2012).

In recent years, computational methods are also used besides experimental works to understand the nature of the chemical reactions. For instance, density functional theory (DFT) utilizing quantum chemical calculations, gives information about accurate energy and geometry calculations as well as reaction barriers at atomic/molecular level (Liu *et al.*, 2011).

The aim of the current study is designing a vibrational frequency data base for CDRM reactants, products and intermediate species on Co(111) flat surface, Ni(220) and NiPt (220) terraced surfaces at atomic scale through using Density Functional Theory (DFT) Calculations. $DMol^3$ tool of Materials Studio codes were used in these calculations. Vibrational frequencies of CH_x(x=0-4), CO_2, CO, O, and H were investigated on Co(111),

Ni(220) and NiPt(220) geometries for which their presence in the Co- and Ni- based catalyst prepared by our group, had been previously determined by XRD analysis.

Chapter 2 includes literature survey for CDRM reaction, catalysts used for CDRM reaction in experimental and computational studies, frequency analysis on Ni and Co based catalysts. In chapter 3, theoretical background of DFT and computational methodology that applied in this study are introduced. The results acquired are presented and discussed in Chapter 4. Conclusions of this study and recommendations for future studies are demonstrated in Chapter 5.

2. LITERATURE SURVEY

Hydrogen is considered as the future clean energy source and carrier. Fossil fuels, water through either splitting or electrolysis, and biomass are used for hydrogen production (Fechete *et al.*, 2012). Hydrogen is produced mostly by steam reforming of natural gas. Steam reforming of liquid hydrocarbons, catalytic partial oxidation, autothermal reforming, methanol steam reforming are alternative ways of hydrogen production. However, use of fossil fuels causes CO_2 emission (Rostrup-Nielsen, 2004). CO_2 is one of the greenhouse gases and considered as the main reason of global warming and climate change. CO_2 can be converted to useful products by reverse water-gas shift, hydrogenation, and through reactions with hydrocarbons (Fechete *et al.*, 2012).

2.1. Carbon Dioxide Reforming of Methane Reaction and its Mechanism

Catalytic Dry Reforming of Methane (CDRM) is a reaction that used the two main greenhouse gases (CH_4 and CO_2) and produces synthetic gas, a mixture of H_2 and CO, with a H_2/CO ratio close to one. Furthermore, it utilizes natural gas resources with high amount of CO_2, and it refrains costly and complicated separation processes (San-José-Alonso *et al.*, 2009). In addition, biogas that contains methane, carbon dioxide and traces of hydrogen sulfide can be also used as a CDRM feed for hydrogen production (San-José-Alonso *et al.*, 2009; Xu *et al.*, 2009). Low H_2/CO ratio is beneficial for Fisher-Tropsch synthesis for manufacturing liquid hydrocarbons (Zeng *et al.*, 2012). However, CDRM is an endothermic reaction and needs high reaction temperature that may lead to both sintering of metals and loss of catalyst activity due to formation of carbonaceous species on the active sites (Zeng *et al.*, 2012; Meshkani and Rezaei, 2011).

CDRM has a complex reaction network rather than being an independent reaction. Reactions from 2.2-2.7 can be occurred at the CDRM reaction conditions. These seven reactions can be reduced to three stoichiometrically independent reactions by Aris method. These three independent reactions are 2.1, 2.2 and 2.7 or 2.2, 2.5 and 2.6 (Mark *et al.*, 1997).

$$CH_4 + CO_2 \leftrightarrow 2CO + 2H_2$$ methane reforming (2.1)

$$CO_2 + H_2 \leftrightarrow CO + H_2O$$ reverse water gas shift (2.2)

$$CO_2 + 4H_2 \leftrightarrow CH_4 + 2H_2O$$ methanation (2.3)

$$CH_4 + H_2O \leftrightarrow CO + 3H_2$$ steam reforming (2.4)

$$C + CO_2 \leftrightarrow 2CO$$ Boudouard reaction (2.5)

$$CH_4 \leftrightarrow C + 2H_2$$ CH_4 decomposition (2.6)

$$C + H_2O \leftrightarrow CO + H_2$$ coal gasification (2.7)

Mark and coworkers studied Ir/Al_2O_3 catalyst in the reaction temperature range of 700-850 ^oC to find out the kinetics of CDRM for stoichiometric feed compositions. In this temperature range, the stepwise model had the best fit whereas Langmuir-Hinshelwood or Eley Rideal type models were not found valid in the whole temperature range. In stepwise model, decomposition of the methane is the rate-determining step, and then active surface carbon reacted with gaseous CO_2 to give 2CO (Mark *et al.*, 1997).

Zhang and Verykios (1994) have performed kinetic studies on $Ni/\gamma\text{-}Al_2O_3$, CaO promoted $Ni/\gamma\text{-}Al_2O_3$ and Ni/CaO catalysts. CaO addition to the $Ni/\gamma\text{-}Al_2O_3$ resulted in higher activity and stability. Langmuir-Hinshelwood model was applied to explain kinetics of CDRM having dehydrogenation of methane as the rate-determining step.

$Ni/\gamma\text{-}Al_2O_3$ was used in another study for CDRM. Activation energy of CO production was computed as 80 kJ/mol and this value was higher than those calculated for consumption of CH_4 and CO_2. The work on CDRM kinetics revealed that the best model is Langmuir-Hinshelwood model kinetics having CO formation as the rate-determining step. In the recommended mechanism, firstly methane dehydrogenation occurred than surface carbon react with adsorbed CO_2 to give 2CO (Wang and Lu*,* 1999).

Kinetic studies for CDRM were carried out on $Ni/La/\alpha\text{-}Al_2O_3$. The findings from experiments were in agrement with Langmuir-Hinshelwood model, which surface reaction was the rate-determining step, or Eley-Rideal mechanism in which the reaction between CH_x and $CO_{2,g}$ was the rate-determining step at low partial pressure of CO_2, whereas at high partial pressure of CO_2 adsorption of CH_4 was the rate-determining step. Activation energy for CDRM was computed as 90 kJ/mol (Olsbye *et al.*, 1997).

Mechanism of CDRM was examined over Rh supported on Sr-doped hexaaluminate. In the mechanism of CDRM, surface oxygen came from dissociation of HCO^*, which was produced by the reaction between CO^*+H^* (McGuire *et al.*, 2011). On the contrary, Rostrup-Nielsen and Bak-Hansen (1993) suggested a mechanism for CDRM that surface carbon produced by methane dehydrogenation reacted with surface oxygen produced by dissociation of CO_2.

2.2. Catalysts for CDRM Reaction

Catalytic Dry Reforming of Methane (CDRM) is a highly endothermic reaction. Severe reaction temperature causes coke deposition, and sintering of the metallic phase and the support. Therefore, there are lots of studies to explore catalysts with better activity, selectivity and stability for production of syngas through CDRM (Özkara-Aydınoğlu and Aksoylu, 2011).

Nature of active sites, as well as their acidity/basicity, and the acidity/basicity of support affect the activity and stability of CDRM catalysts. On a strongly basic support, CO_2 adsorbed on the surface, and reacts with surface carbon; on the other hand, strongly acidic support cause coke deposition (Ni *et al.*, 2012).

Noble metals like Pt, Rh and Pd have been considered as good candidates for catalyzing CDRM, in terms of their activity and stability. Nevertheless, they are too costly to be used in industry and have low availability (Meshkani and Rezaei, 2011; Özkara-Aydınoğlu and Aksoylu, 2010; San-José-Alonso *et al.*, 2009; Zeng *et al.*, 2012).

Rostrup-Nielsen and Bak Hansen (1993) analyzed the activity of Ni, Ru, Rh, Pd, Ir and Pt. They discovered that Ru and Rh have presented the highest catalytic activity (Rostrup-Nielsen and Bak Hansen, 1993). Rhodium has the best catalytic activity and stability for the CDRM, but it has high price and low availability. On the other hand, IB metals (Cu, Ag and Au) are found having much higher methane dissociation enthalpies and therefore poorly active in methane chemisorption (Djinović *et al.*, 2012).

Pt enhances the catalyst stability for CDRM reaction. Alumina supported Pt with metal oxides promoters, such as ZrO_2, MgO, Al_2O_3, La_2O_3 and CeO_2, present very good stability. For instance, zirconia has an acidic-basic surface with redox ability. Thus, forming solid solution can create oxygen vacancies. Consequently, zirconia advances oxygen mobility and thus carbon deposits can be oxidized easily (Carvalho *et al.*, 2014).

Carvalho and coworkers studied mesoporous alumina supported Pt or Ru catalysts that are promoted by MgO, ZrO_2, CeO_2 or La_2O_3 in CDRM reaction. At 650 ^oC and CH_4/CO_2 molar ratio of 1, Pt containing CeO_2- Al_2O_3 exhibited higher catalytic activity and stability in contrast to other catalysts. Activity and stability of the catalysts at different temperatures and molar ratios have been also investigated. While increasing temperature enhances the Pt-based catalysts activity, it decreases activity of the Ru-based catalysts. At different molar ratios, methane is fully oxidized on Pt based catalysts, and partially oxidized on Ru (Carvalho *et al.*, 2014).

Ce promoted Pt/ ZrO_2 catalysts were tested between 773 and 973 K with CH_4:CO_2 ratio of 1:1. Activity and stability of the catalysts were explored via changing preparation parameters and cerium loading. The highest activity and stability is obtained from 1 wt.% Ce coimpregnated Pt/ZrO_2 catalyst. When CH_4:CO_2 ratio changes from unity to 2:1, 1 wt.% Pt–5 wt.% Ce /ZrO_2 showed the best stability (Özkara-Aydınoğlu *et al.*, 2009).

Ni/SiO_2, Rh/SiO_2 and Ni-Rh/SiO_2 catalysts were investigated for CDRM. Catalysts were prepared by incipient to wetness impregnation method. The reaction temperature was increased from 300^oC to 850^oC during tests. Consumption of CH_4 increased with increasing temperatures and at 850^oC almost 100% conversion was obtained. For all catalysts conversion displayed the same trend. Thus, someone could interpret that SiO_2 supported Ni, Rh and Ni–Rh catalysts were all useful catalysts for CDRM. Moreover, Rh consisted catalysts had high stability (Jóźwiak *et al.*, 2005).

1 wt% Pt loaded catalysts supported on ZrO_2, CeO_2, and CeO_2-ZrO_2 with different amount of CeO_2, were prepared in order to elucidate the support effect in the CDRM reaction. Catalysts were characterized using X-ray diffraction (XRD), Raman and X-ray photoelectron spectroscopy (XPS), temperature-programmed reduction (TPR) and thermo

gravimetric analysis (TGA). Reaction was performed at 823 K and activity of catalysts was investigated. Methane conversion activity series were found as: Pt/ZrO_2 > $Pt/1CeO_2–ZrO_2$ ≈ $Pt/3\ CeO_2–ZrO_2$ > $Pt/6\ CeO_2–ZrO_2$ > $Pt/12\ CeO_2–ZrO_2$ > $Pt/\ CeO_2$. CeO_2 addition up to 6wt% was found to be stabilized the catalysts and prevented Pt particles from coke deposition (Damyanova *et al.*, 2009).

General formula of pyrochlores is $A_2B_2O_7$; there transition metals place at B site and large cations place at A site. Pakhare *et al*. used lanthanum zirconate ($La_2Zr_2O_7$) pyrochlores, LRuZ with 2wt.% Ru and LPtZ with 3.78 wt.% Pt in CDRM reaction. Activity of the catalysts was analyzed at 525 ^oC, 575 ^oC and 625 ^oC for 600 min time-on-stream (TOS). Activation energies calculated based on methane and carbon dioxide were lower for LRuZ than that for LPtZ. Methane conversion increased with reaction time for LPtZ and LRuZ, and conversion of CH_4 and CO_2 on LRuZ was higher than that over LPtZ. H_2/CO product ratio for LPtZ was lower than LRuZ at all temperatures. Carbon formation decreased with increasing temperature according to Temperature Programmed Oxidation (TPO) results obtained from the analysis of the spent catalysts (Pakhare *et al.*, 2013).

Temperature programmed CDRM reaction was studied over 2% Rh-CeO_2 that was prepared by hard-template method. Below 623K there was no catalytic activity, however with increasing temperature, catalytic activity was increased, and at 1073 K, 87% methane and 93 % CO_2 conversions were obtained. Methane conversion was lower than CO_2 conversion due to reverse water gas shift (RWGS) reaction. Below 973 K, RWGS used hydrogen, and above 973 K 2% Rh-CeO_2 catalyst produced syngas with a ratio close to 1. 21 h TOS stability test at 923 K showed that catalyst was stable, however 70 h TOS stability test at 1023 K presented loss of activity, due to catalyst sintering (Djinović *et al.*, 2012).

Pillared layered clays (PILC) are used as supports and lead to well dispersion of metal particles. 3.5% or 10% Me/Al-PILC catalysts, where Me is Ni, Rh, Pd or Ce, were synthesized by impregnation method. The conversion of CH_4 and CO_2 at 650°C followed the trend of Rh ≈ 10% Ni >> Pd > 3% Ni >>Ce. Coke deposition was found very low on these catalysts except 10% Ni/Al-PILC. H_2/CO ratio was found more than 1 for Rh, and it declined with a sequence Rh (1.11) > Pd (0.84)>>Ni, Ce (0.12–0.05) (Barama *et al*, 2009).

Activated carbon (AC) has low cost, high surface area and high resistance to sulfur. Activated carbon based catalysts are studied for CDRM. AC, AC-HNO_3 and AC-$NaNO_3$ catalysts are investigated at 700-1000°C. At 700°C, activity of these catalysts is low and different from each other, but at 1000°C their activity is very high and akin. In addition, the molar H_2/CO product ratio rises with temperature for all catalysts. H_2/CO mole ratio over AC-HNO_3 was close to 1 comparing the other two catalysts. According to FTIR, the hydroxyl groups were crucial for CDRM on AC. AC-$NaNO_3$ hinders carbon deposition and AC-HNO_3 is useful for methane decomposition (Xu *et al.,* 2014).

2.3. Ni based Catalysts for CDRM

The main problem of Ni-based CDRM catalysts is the carbon deposition and sintering (Akpan *et al.,* 2007). Surface structure and the acidity/basicity play a crucial role on coke deposition for Ni- based catalysts. If Ni particles disperse efficiently on support and be in the size of less than 6 nm, formation of carbon may reduce. Support with a property of basicity improves the reaction of CO_2 with surface carbon (Ni *et al.*, 2012).

2.3.1. Experimental Studies

Alumina supported Ni-based catalysts are investigated mostly for CDRM reaction. Sintering of Ni on alumina leads to deactivation and thus carbon fouling occurs on the surface. Ni/MeO_x-Al_2O_3 catalysts, where Me is CeO_2, MgO, La_2O_3 or ZrO_2, were prepared with sol-gel method, which is considered making alumina supported catalysts more stable. Addition of CeO_2 decreased the coke on the surface by helping to transfer of oxygen. Addition of La_2O_3 increased the activity of the catalyst in first 3h TOS, but then the catalyst became deactivated, mostly because of high amount of CO and H_2. Ni/ ZrO_2-Al_2O_3 catalyst was stable, and Ni/MgO-Al_2O_3 catalyst has the highest methane and CO_2 conversion (de Sousa *et al.*, 2012).

5 wt% Ni catalysts supported with 0 wt%, 1 wt%, 5 wt%, 10 wt% borated alumina are studied for CDRM reaction. Increase of B_2O_3 amount in the catalysts results in larger Ni particle size. Strong Lewis acid sites are formed on the 5%Ni/1% B_2O_3-Al_2O_3 and 5%Ni/10% B_2O_3-Al_2O_3 catalysts surfaces causing the growth of carbonaceous deposits.

However, weak Lewis acids and OH groups are formed on the 5%Ni/5% B_2O_3-Al_2O_3, therefore this catalyst exhibits better activity and stability by promoting to gasification of carbon. In addition, Ni and coworkers proposed a CDRM mechanism for these catalysts. They thought that CH_4 and CO_2 decompose on the surface and produce CO. Reaction between CH_x and OH species produce CO and H_2 and thus coke does not occurred on the surface (Ni *et al.*, 2012).

NiMgAlLa mixed-oxide CDRM catalysts were prepared by calcining hydrotalcites Conversion of methane and CO_2 increased with increasing temperatures. Lanthanum added catalysts exhibited higher catalytic conversion than not La-doped one, as lanthanum led to formation of carbonates increasing the basicity, and thus CO_2 reacted with CH_x faster. Furthermore, lanthanum addition led to a well Ni dispersion. The catalyst that has the highest La% presented the highest activity. La addition to NiMgAl mixed oxide made catalysts more stable (Yu *et al.*, 2012).

Akpan et al. studied Ni/CeO_2-ZrO_2 catalyst and carried out kinetic, experimental, modeling and simulation studies. Kinetic experiments are performed for different temperatures and feed flow rates. They proposed a kinetic model based on Eley-Rideal (ER) formulation, for which decomposition of methane was the rate-determining step. They used pseudo-homogenous, 2-D, non-isothermal model for the CDRM reaction. Their model was compared with experimental data and they attained good agreement (Akpan *et al.*, 2007).

1.5- 2.5 wt% K was added to 19%Ni/MgO catalyst in order to investigate the activity and the stability of the catalyst at 650°C and compared with that of the unpromoted 19%Ni/MgO. Ni/MgO catalyst was synthesized by incipient wetness method and K was added by wet impregnation. Although addition of K lowered the CDRM activity, it improved the stability of the catalysts. Furthermore, apparent activation energy was increased from 50kJ/mol to the 70kJ/mol by addition of K due to alteration in the electronic and geometric characteristics (Frusteri *et al.*, 2001).

Syngas production via CDRM reaction was investigated on the nanocrystalline MgO supported Ni catalysts having different Ni loadings. In the tests, Ni loading, GHSV, and

feed ratio were used as the experimental parameters. 5wt%Ni/MgO, 7wt%Ni/MgO, 10wt%Ni/MgO, and 15wt%Ni/MgO catalysts were prepared and characterized. For all samples, activity of catalyst was increased with increasing temperature. While 7wt%Ni/MgO catalyst showed the highest CH_4 and CO_2 conversions and the highest H_2 and CO yield, 15wt% Ni/MgO catalyst exhibited the lowest conversion and yield, because of its very low Ni dispersion. All catalysts with various Ni loading were stable for 300 min at 700 °C. Increasing GHSV declined the CH_4 and CO_2 conversion of 5wt%Ni/MgO catalyst, at CO_2/CH_4 feed ratio 1:1 and 700°C. Increase in the CO_2/CH_4 feed ratio on 5wt%Ni/MgO catalyst at 700 °C led to occurrence of WGS reaction and raised CH_4 conversion (Meshkani and Rezaei, 2011).

2.3.2. Computational Studies

Density functional theory (DFT) was used for examining the CH_4 dissociation on Ni(111), Ni(100) and Ni(110) surfaces (Wang *et al.*, 2006). CH_x adsorptions were studied using GGA and Perdew-Burke-Ernzerhof (PBE) functional and Cambridge sequential total energy package (CASTEP). The local density of states (LDOS) profiles were obtained to interpret electronic structures of adsorbed CH_x. LDOS of CH_x are alike on Ni(111), Ni(100) and Ni(110) surfaces. Thermodynamically, Ni(100) is the most desirable surface for CH_4 dissociation in contrast with Ni(111) and Ni(110). Carbon formation is very easy on Ni (100) surface, thus CO formation and coke deposition in CDRM systems probably occurred. In other words, Ni (100) was found having high reactivity but low stability for CDRM reactions.

CO_2 chemisorption on the Ni(111), Ni(100), and Ni(110) surfaces was analyzed with density functional theory using CASTEP with GGA-PBE functional. CO_2 chemisorption preference was in the order of Ni(110) > Ni(100) >Ni(111). Dissociative adsorption of CO_2 was preferred by the surfaces in the order of Ni(100) > Ni(111) > Ni(110) thermodynamically (Wang *et al.*, 2005).

Zhu and coworkers (2009) investigated the reaction mechanism of CDRM on Ni(111) using spin polarized DFT. In their work, they utilized the Vienna ab initio simulation package (VASP) with projector augmented wave (PAW) method and

generalized gradient approximation (GGA) in the formulation of PBE functional. Firstly, the adsorption energies of species, which may form during CDRM, were computed and transition states of elementary steps were found by dimer method. CO_2 decomposition, the dissociation of CH_4, oxidation of CH and H, and the decomposition of CHO(H) and COH were explored to get an idea about reaction mechanism. CO_2 was dissociated to CO and O via a direct pathway. This atomic O oxidized CH and C, which were formed by the dissociation CH_4. They proposed that oxidation of CH and C was the dominant reaction pathway and affected the overall reaction rate, although dehydrogenation of CH_4 was the rate-determining step (Zhu *et al.*, 2009).

Decomposition of CH_4 was investigated on Ni(100), Ni(111) and Ni(553) surfaces by DFT calculations using the program ADF-BAND on SHARCNET. In the spin unrestricted calculations, revised PBE and GGA functional was used. On Ni (111), the CH_x (x = 0–3) and H species were adsorbed at the threefold hcp sites. On the Ni (1 0 0) surface, the hollow site was found as the favorable site for the CH_4, CH_2, CH and C adsorption. CH_3 and H were chemisorbed at the bridge sites. On the Ni(553), the preferred adsorption sites for CH_3 and CH_2 were the bridge sites along the step edge while the favorite site for CH and H adsorption was hcp site on the terrace behind the step edge. Moreover, H adsorbed on the upper terrace on the fcc site. Adsorption energy of the carbon atom on the surfaces was in the order of Ni (1 0 0) > Ni (5 5 3) > Ni (1 1 1). While dissociation of CH into the C and H was the rate-limiting step on Ni (111), decomposition of CH_4 to the CH_3 and H was found to be the rate-limiting step on Ni (1 0 0) and Ni (5 5 3) (Li *et al.*, 2012).

DFT calculations were performed on Ni(111), Ni(211), Ni_3C(001) and Ni_3C(111) surfaces for CDRM using VASP with GGA-PBE functional and PAW method. Firstly, CH_4 dissociation with its elementary steps was investigated on flat and stepped surfaces of Ni and Ni_3C. Ni_3C(001) was the favorite surface for methane dehydrogenation. During transition state search, CH_3 adsorbed on atop site and H was adsorbed on threefold hollow site of Ni(111) and Ni_3C(001), and on the bridge sites of Ni(211) and Ni_3C(111). For CH_3 dissociation Ni_3C(111) was the least preferred surface. During dissociation of CH_3, CH_2 was adsorbed on fcc site and H adsorbed on the atop site of flat surfaces. On the other hand, CH_2 was adsorbed on the bridge sites and H adsorbed on atop sites of stepped

surfaces. Ni(211) surface was discovered to be the favorite surface for CH_2 dehydrogenation to CH+H. CH was located on the fcc site of flat surfaces and on the bridge5 (B_5) site of the stepped surfaces, while H was located on bridge sites of both flat and stepped surfaces. For CH dissociation, Ni(111) surface was found as the least preferred surface on the basis of activation energy barrier calculated. CH dehydrogenation was encountered as structure sensitive. Direct dissociation of CO_2 was also considered on this work and Ni(111) surface was found to be the least preferred surface, while CO_2 dissociation on Ni_3C surfaces was found favorable. In the transition state, CO was adsorbed on atop site and lower part of B_5 site of flat surfaces and stepped surfaces, respectively. O was adsorbed on bridge site of flat surface, and on the upper part of B_5 site of stepped surfaces. Although oxidation of CH and C was adverse on all surfaces, dissociation of CHO to CO+H was detected to be preferred on all four surfaces. Upon kinetic analysis, CH oxidation and the CO dissociation affected the coke deposition on the surface. Moreover, flat Ni surfaces had best activity and carbon resistance (Wang *et al.*, 2014).

2.4. Co based Catalysts for CDRM

Co-based catalysts are considered as alternative to Ni-based catalysts for CDRM reaction (Baouarab *et al.*, 2004). Cobalt is highly active, available and has low price. Unfortunately, its activity is reduced due to sintering, metal oxidation, formation of inactive chemical species, and growth of coke deposits (Alonso *et al.*, 2011).

2.4.1. Experimental Studies

Activity and stability of Co/γ-Al_2O_3 catalyst in CDRM were examined in a study for which Co loading and calcination temperature were used as the parameters. Catalysts that were calcined at 500 °C had larger BET surface area, compared the ones that were calcined at 700°C. CDRM reaction was performed at 900°C. Among the catalysts that were calcined at 500 °C, serious deactivation was observed on 2 wt% Co/γ-Al_2O_3 and 20 wt% Co/γ-Al_2O_3, although on 6, 9 and 12 wt% Co/γ-Al_2O_3, no deactivation was observed for 50h TOS. 9 wt% Co/γ-Al_2O_3 catalyst calcined at 700°C was the most stable one among others. No coke deposition was observed on 2 wt% Co/γ-Al_2O_3 catalyst that was calcined

at 1000 °C, but it lost its activity because of oxidation of its active metal sites (Ruckenstein and Wang, 2002).

Co/ZrO_2 catalyst was doped with La, Ce, Mn, Mg or K to increase its resistance to carbon formation. The CDRM reaction performed on $Co\text{-}X/ZrO_2$ (X=La, K, Mn, Mg, Ce) at 923 K and 1:1 CH_4/CO_2 feed ratio for 6 h TOS at 1 atm. CH_4 conversion order was obtained as Ce > none > La ≈ Mn > Mo > K > Mg. $Co\text{-}Ce/ZrO_2$ catalyst also exhibited highest H_2 and CO yield. Although Co/ZrO_2 catalyst was deactivated at the end of 6h TOS, $Co\text{-}La/ZrO_2$ catalyst was still stable. $Co\text{-}Mn/ZrO_2$ catalyst lost its 20% of its activity at the end of 6h TOS. $Co\text{-}Mg/ZrO_2$ and $Co\text{-}K/ZrO_2$ catalyst show very low activity and stability compared the other samples, due to coke formation and sintering of cobalt metals. Furthermore, effect of space velocity on the most active and stable catalysts, i.e. $Co\text{-}Ce/ZrO_2$ and $Co\text{-}La/ZrO_2$, was searched and it was found that decrease in space velocity result in a rise in the activity of both catalysts (Özkara-Aydınoğlu and Aksoylu, 2010).

10 wt% Co/Al_2O_3 catalyst was prepared and calcined at 773 K and 973 K to obtain different surface structures, which are (5 0 0) and (7 0 0), respectively. 0.1 or 0.5 wt% Rh were added to this catalyst. Interaction of methane, CO_2 and CH_4+CO_2 mixture with the catalyst was investigated via in situ-DRIFT analysis. The catalyst that calcined at 973 K was found more active than that calcined at 773 K. CO production rate was in the order: 0.5%Rh + 10% Co/Al_2O_3 (5 0 0) > 0.1%Rh + 10% Co/Al_2O_3 (5 0 0) > 10% Co/Al_2O_3 (5 0 0). At (5 0 0) bare surface, the growth of carbon was higher than that on (7 0 0) bare surface. However, Rh added catalyst samples exhibited the opposite behavior (Ferencz *et al.*, 2014).

5, 10 or 35 wt % MgO was added to 5 wt%Co/SiO_2 CDRM catalyst. Addition of MgO caused to form Mg_2SiO_4 and thus metal was dispersed efficiently and Co sintering was hindered. Methane and CO_2 conversion raised as temperature increased from 500 to 800 °C. Basicity of support provided surface oxygen and thus surface carbon react with it and formed CO (Bouarab *et al.*, 2004). In another study of Bauarab *et al.* (2005), La_2O_3 was added to $Co(O)/SiO_2$ and the effect of basicity/acidity of the catalyst on CDRM activity was searched. Addition of highly amount of lanthanum oxide made catalyst more basic and prevented the carbon formation.

K and Sr were coimpregnated on alumina supported Co catalyst to carry out CDRM reaction. Optimum K amount was found as 0.6 wt% for 0-5 wt% loading range. Although carbon formation was declined, activity of the catalyst was affected negatively with the increase in the amount of K. Coke deposition was hindered, because potassium obstructed CDRM and methane decomposition, and also promoted the oxidation of surface carbon. On the other hand, active sites in the 5wt%K added catalyst became larger and led to a decline in the activity of the sites (San-José-Alonso *et al.*, 2011).

2.4.2. Computational Studies

A DFT study was carried out for CH_x (x=0-4) adsorption and CH_4 dehydrogenation on Co (1 1 1) surface. CASTEP in Material Studio with GGA and Perdew and Wang (PW91) functional was used for spin polarized DFT calculations. According to energy analysis, decomposition of CH_4 was occurred in an order like $CH_4^* \rightarrow CH_3^* + H^* \rightarrow CH_2^* + 2H^* \rightarrow CH^* + 3H^* \rightarrow C^* + 4H^*$. CH_3 and H favored to adsorb on threefold hollow hcp and fcc sites of Co(1 1 1) , respectively. In addition, CH_2, CH and C favored to adsorb on hcp sites of Co(1 1 1). Adsorption energies of CH_x(x=0-4) and H were calculated and obtained in the following order: $CH_4 < CH_3 < H < CH_2 < CH < C$. In accordance with optimized transition state form, decomposition of CH_4 to CH_3 and H was attained to be the rate-determining step. CH_2 can be easily hydrogenated to CH_3 and dehydrogenated to CH based on its reported forward and backward reaction energy barriers. Moreover, CH dehydrogenation had high-energy barrier and demonstrated that it was kinetically and thermodynamically adverse (Zuo *et al*., 2010).

CO_2 adsorption on Co(111), Co(100), Co(110) was investigated by using DFT calculations of VASP program, applying GGA- PW91 functional and PAW method. During geometry optimization, CO_2 was bent from its linear form. Adsorption of CO_2 on Co(111) was found endothermic, while it was exothermic on other surfaces. CO_2 adsorption energies on Co was acquired in the following order: Co(110)>Co(100)>Co(111), indicating that Co(110) surface was the most preferred one. LDOS profiles of free CO_2, CO_2 chemisorbed on Co, and d orbital of CO_2 demonstrated the existence of charge transfer to CO_2 from the Co surface (de la Peña O'Shea *et al.,* 2008).

CH_x (x=0-4) adsorption and CH_4 dehydrogenation on Co (0 0 0 1) surface was studied by using DFT calculations via CASTEP program utilizing GGA-PW91 functional. CH_4 adsorption energy on Co was found very low, indicating that chemisorption did not occur. Highest adsorption energy was calculated for C adsorption. Adsorption of CH_3, and H was found favorable on the three fold fcc hollow sites, while CH_2, CH, and C was found to prefer three fold hollow hcp sites. According to optimized transition state form for methane dehydrogenation, CH_3 can be easily dehydrogenated to CH_2, and dehydrogenation of CH_2 to CH or hydrogenation of CH to CH_2 also took place easily. Elementary step, which was $CH_4^* \rightarrow CH_3^* + H^*$, was determined to be the rate-determining step (Huang *et al.*, 2012).

CO adsorption study on Co (0 0 0 1) was performed utilizing spin-polarized DFT calculations and VASP with GGA- revised PBE (RPBE) functional. Adsorption energy of CO was found greater on atop site showing atop site was the favorable site at 0.33 ML surface. C-O stretching frequency and C-metal frequency were the largest on atop site. During CO adsorption, superior interactions appeared from 5σ and 2π orbitals of CO. On atop site, CO affected the magnetization of the surface mostly among other sites (Ma *et al*., 2008).

2.5. Bimetallic Catalysts for CDRM

Bimetallic catalysts display different electronic and chemical features from those of their parent metals. Firstly, creation of heteroatom bonds alters the electronic structure of the metal surface through ligand effect. Secondly, change in the average length of metal-metal bond in bimetallic catalysts causes the strain effect, and electronic structure is reshaped through alteration in orbital overlap. Thus, catalysts with better activity, selectivity and stability can be achieved (Yu *et al*., 2012). Ni based bimetallic catalysts attracts attention mostly for CDRM. Active metals are dispersed efficiently in bimetallic systems (Del Santo *et al.*, 2012).

2.5.1. Experimental Studies

Addition of noble metals to Ni catalysts increases its resistance to carbon formation. Catalytic activities of bimetallic Pt(0.5%)-Ni(10%)/Al_2O_3 catalyst was investigated and compared with these of Ni(10%)/Al_2O_3 and Pt(0.5%)/Al_2O_3. Ni(10%)/Al_2O_3 catalyst presented high activity at 750^oC, however Pt(0.5%)/Al_2O_3 deactivated due to sintering. Better activity was obtained on Pt(0.5%)-Ni(10%)/Al_2O_3 (Miguel *et al.*, 2012).

Pt-Ni/Al_2O_3 catalysts having different loading ratios were prepared and tested for their activity and stability in CDRM. 0.3Pt–10Ni, which has the lowest Ni/Pt ratio tested, displayed the best catalytic activity and stability for production of syngas. When oxygen or water was introduced to the feed having CH_4 and CO_2, changes in activity and stability characteristics were observed. The results from DRM+POX demonstrated that reaction mechanism is related to Pt loading and Ni/Pt ratio of the catalysts. DRM+SR reactions resulted in coke formation on low-Pt loaded catalysts (Özkara-Aydınoğlu and Aksoylu, 2011).

Luisetta and coworkers worked on Co-Ni/CeO_2 catalysts for CDRM. Reaction took place at 600-800 ^oC with 1:1 CH_4:CO_2 feeding ratio. Co-Ni/CeO_2 catalyst exhibits better activity than those of Co/CeO_2 and Ni/CeO_2. CH_4 conversion was 50% at 600^oC and 97% at 800 ^oC. H_2/CO selectivity series was found as Co-Ni/CeO_2> Ni/CeO_2> Co/CeO_2. Co-Ni/CeO_2 and Co/CeO_2 display higher stability than Ni/CeO_2 (Luisetto *et al.*, 2012).

Ni-Mo/SBA-15 bimetallic CDRM catalysts were synthesized by using incipient to wetness co-impregnation method having 12wt% Ni and 0, 0.3, 0.5, and 0.7 Mo/Ni atomic ratios. In the beginning of the reaction conducted at 800 °C, CH_4 conversion on these catalysts was in the following order: 1Ni(97.2%) > 0.3Mo1Ni(95.5%) > 0.5Mo1Ni(94.3%) > 0.7Mo1Ni(94.1%). The reason why monometallic Ni catalyst showed highest activity was proposed as great BET surface area and large number of active sites. However, it lost its activity after 60h TOS and the most stable catalyst was found as 0.5Mo1Ni/SBA-15, which had a 94% conversion even after 250h TOS stability test. Moreover, Mo_2C species were formed during reaction and protected catalysts from coke formation and Ni sintering (Huang *et al*., 2011).

CDRM reaction was carried out on Al_2O_3 and ZrO_2 supported Ni and bimetallic Pd(or Pt)Ni catalysts. Temperature programmed procedure was utilized for decomposition of CH_4 and CO, and CDRM reaction. It demonstrated that carbon formation occurred through either CH_4 or CO. Alumina supported catalysts were less active than zirconia supported catalysts. Bimetallic catalysts were more stable than monometallic Ni catalyst. $NiPd/ZrO_2$ considered to be applicable for industry (Menegazzo *et al.*, 2012).

2.5.2. Computational Studies

A periodic density functional theory (DFT) was used for analyzing the decomposition of methane on Pt(111), Ir(111) and PtIr(111) surfaces. All calculations were performed via using CASTEP tool of Materials Studio 5.0 with GGA-PBE functional. The transition state was located by using the linear synchronous transit/quadratic synchronous transit (LST/QST) method. On Pt(111) surface, CH_4 and CH_3 were preferably adsorbed at atop sites, while CH, C, and H species were adsorbed on the fcc sites. On Ir(111) surface, the most favorable site for CH_4, CH_3 and H adsorption was found as the atop site, whereas CH_2 chemisorbed favorably at the bridge site, and CH and C adsorbed on the hcp hollow site. On the PtIr(111) surface, the similar trend was observed but CH and C species preferred the fcc hollow site. Dehydrogenation of CH_4 into the CH_3 and H was found as the rate-determining step for PtIr(111) and Ir(111) surfaces (Qi *et al.,*2013).

Another density functional theory work was performed for analyzing adsorption of CH_4, CH_3, CH_2, CH, C, H and dissociation of CH_4, CH_3, CH_2, CH on the (111) surface of NiCo alloy. DFT calculations were done by using CASTEP utilizing GGA and PBE functional. The results obtained were comparatively analyzed with the data obtained on Ni(111) surface. CH_x and H were adsorbed on threefold hollow site on NiCo(1 1 1), similar to on Ni(111). The dehydrogenation of CH_x occurred on Co atop, rather than Ni atop. Rate-determining step was found as $CH_4 \rightarrow CH_3+H$ dehydrogenation step on NiCo; while for pure Ni, it was $CH \rightarrow C+H$ dehydrogenation step (Liu *et al.*, 2011).

Liu and his coworkers studied CH_4 dissociation mechanism of on NiCu(111) based on 2 surface models. One model (Model A) had of Ni/Cu ratio 1, and the other model (Model B) was built changing one surface Ni atom with Cu atom in the Model A.

CH_x(x=0-3) was stable at the threefold sites having two Ni and one Cu atoms on Model A. On the other hand, on Model B, CH_x(x=0-3) was stable at the threefold sites with one Ni and two Cu atoms at its legs. The lowest adsorption energy of C was obtained on Model B, indicating that adsorption is the most stable on Model B. Dissociation of CH to the C and H was determined as the rate-determining step for both models (Liu *et al.*, 2012).

Main problem of the non-noble metal catalysts is coke formation during CO_2 reforming of methane. Using CASTEP program in Material Studio (4.4), adsorption energies of CH_x (x=0-4) and dehydrogenation of CH_4 were calculated on Fe, Co, Ni, Cu, NiFe, NiCo and NiCu metals. Transition states were investigated using LST/QST complete method via DMol3. All calculations were done on the (111) surfaces. Furthermore, activation and reaction energies with d-band center of the metallic surfaces were computed. During kinetics analysis, the sequence of C coverage amount on the catalyst surface at 875 K were found as: Cu < NiCu(S)< NiCu < Co < Fe < NiCo < Ni < NiFe. According to this order, coke formation occurs mostly on NiFe bimetallic catalysts and the least on segregated NiCu (Liu *et al.*, 2013).

The mechanism of CH_x (x=0-4) dehydrogenation on NiPd(111) was investigated by using DFT calculations utilizing VASP and GGA-PBE functional. Ni-Pd alloy consisted 1:1 Ni/Pd ratio. Hollow sites with two Ni atoms were found as favorable sites for CH_x(x=1-3) adsorption. CH_X (x = 1–4) dehydrogenation was found more preferable on Ni than that on Pd. CH→ C+H mechanism had the highest energy barrier on NiPd(111) in accordance with TS search. Ni-Pd alloy had greater activity than Ni(111) and Pd(111) (Li *et al.*, 2013).

2.6. Frequency Analysis on Ni- and Co- based Catalysts

Activity and stability of CH_x(x=1-3) on Ni(111) was examined by using DFT and the results were compared with experimental findings. CH and CH_3 preferred to adsorb on three-fold hollow sites, while CH_2 preferred both threefold hollow sites and bridge sites. C-H stretching frequency was found as 3035 cm^{-1}, which was very close to experimental value of 2970 cm^{-1}. Methyl stretching frequency attained as 2730 cm^{-1}, which was also near to experimental value of 2655 cm^{-1} (Watwe *et al.*, 2000).

Vibrational frequency was obtained for stable CO_2 on Co(1 0 0) and Co(1 1 0) by using DFT calculations. On fourfold site of Co(1 0 0), symmetric and asymmetric vibrational frequencies were calculated as 1014 cm^{-1} and 1486 cm^{-1}, respectively. Additionally, symmetric and asymmetric vibrational frequencies on short-bridge site of Co(1 1 0) were computed as 1245 cm^{-1} and 1906 cm^{-1}. There was a relation between the OCO angle and the difference between asymmetric and symmetric vibrational frequencies. As OCO angle became larger the difference was greater (de la Peña O'Shea *et al.,* 2008). During adsorption of CO on Co(0001), vibrational frequency of CO was calculated by using DFT calculations. Vibrational frequency of CO on atop, bridge, fcc, and hcp was acquired as 2005, 1841, 1802 and 1790 cm^{-1}, respectively. These data were in consistence with the literature (Ma *et al.*, 2008).

Bouarab and coworkers measured frequencies of methane and CO_2 on Co/ 35%MgO-SiO_2 by using in situ DRIFT. The C-H vibrational frequency of methane was attained as 3014 cm^{-1}, and CO_2 rotation-vibration P and R bands were obtained at 2360 cm^{-1} and 2340 cm^{-1}. CO vibration was also seen and had vibrational frequency between 2000 and 2200 cm^{-1} beside vibrations of CH_4 and CO_2, when CH_4 and CO_2 flowed over the catalysts, signifying that reaction occurred during the flow of mixture (Bouarab *et al.*, 2004)

Low temperature CDRM was analyzed over Ni-CaO/ZrO_2-La_2O_3. For DRIFTS experiments, CH_4/CO_2/Ar mixture (2:2:16) was used in the tests performed at 773 K. Furthermore, in order to observe behavior of reactants on the catalysts surface, CH_4/Ar and CO_2/Ar also was flowed over the catalyst samples individually. When CH_4/CO_2 mixture was loaded to the system, CH_4 frequency was measured as 3016 cm^{-1} on Ni/ZrO_2-La_2O_3, while it was 2360 cm^{-1} on Ni-CaO/ZrO_2-La_2O_3. CO_2 frequency was obtained as 1305 cm^{-1} on Ni/ZrO_2-La_2O_3, while it was 2345 cm^{-1} on Ni-CaO/ZrO_2-La_2O_3. Moreover, CO frequency was measured as 2181 and 2121 cm^{-1} on Ni/ZrO_2-La_2O_3 and Ni-CaO/ZrO_2-La_2O_3, respectively. After cleaning the surface with Ar, any adsorbed CH_x species were not recognized, meaning the fast reaction is between CH_x and CO_2. However, spectra between 1200 and 1700 cm^{-1} indicated the existence of carbonate on the surface. The bands at 2040 cm^{-1} exhibited that CO was adsorbed on Ni sites linearly. The peak at 1920 cm^{-1} indicated the presence of bridge-bonded CO. When CH_4 was flown over the catalysts and then the

surface was cleaned by Ar, 2931 cm^{-1} and 2860 cm^{-1} frequency data were attained, which were correspond to CH_2 and CH_3 frequencies, indicating the chemisorption of CH_4 on both catalysts. In addition, CO_2 rotation-vibration P and R bands at 2360 and 2340 cm^{-1} were determined on Ni-CaO/ZrO_2-La_2O_3 and Ni/ZrO_2-La_2O_3, respectively (Bachiller-Baeza *et al.*, 2013).

3. METHODOLOGY

3.1. Theory behind Computational Methods

Quantum chemical and molecular mechanics models have been established in order to calculate molecular structure and energetics.

Quantum chemical models arise from Schrödinger equation. It conducts molecules as collections of nuclei and electrons, without any reference to chemical bonds. For more than one electron system, making approximations is needed to solve Schrödinger equation. Quantum chemical models vary in the nature of these approximations that can be classified in terms of their capability, reliability, and cost.

Hartree-Fock approximation is first applied to many-electron Schrödinger equation, and Hartree-Fock molecular orbital models or simply molecular orbital models are then discovered. The Hartree-Fock approximation considers that electrons act as independent particles. Hartree-Fock models describe equilibrium geometries and conformations, good and also accomplish well for various kinds of thermochemical comparisons except where transition metals are included. Hartree-Fock models are failed because of an incomplete description of “electron correlation” or, the way in which the motion of one electron affects the motions of all the other electrons.

Two distinct approaches for development of Hartree-Fock models have come out. First approach utilizes combination of Hartree-Fock descriptions for ground and excited states to build more flexible description of electron motions. Configuration interaction (CI) and Møller-Plesset (MP) models are employed most commonly. The second-order Møller-Plesset model (MP2) is the most practical and widely used one.

The other approach includes an explicit term to account for the way in which electron motions affect each other. In practice, this account is based on an “exact” solution for an idealized system, and is introduced through using empirical parameters. The derived models are referred to as density functional models.

The Hartree-Fock approximation formed also a basis for semi-empirical models, which include additional approximations to simplify the calculations, with minimal unfavorable effect on the results. AM1 and PM3 models are useful for this aim, however this goal has yet to be fully realized.

Molecular mechanics models are an alternative to quantum chemical models. It starts from a chemically reasonable picture of molecular structure. In this idea, molecules are made up of atoms and bonds, and atom positions are adjusted best match to known structural data (bond lengths and angles), and to accommodate non-bonded interactions as well. This is simpler than solving the Schrödinger equation for electron motions, but requires an explicit description of chemical bonding, as well as a large amount of information about the structures of molecules. (Hehre, 2003).

3.1.1. Schrödinger Equation

All quantum mechanical models stem from Schrödinger equation. Schrödinger's wave equation can be written as:

$$\hat{\mathrm{H}}\psi = E\psi \tag{3.1}$$

where ψ is the wavefunction, $\hat{\mathrm{H}}$ is the Hamiltonian operator, E is the total energy of the system (Yates and Johnson, 2007).

Schrödinger equation for the hydrogen atom is as follows:

$$\left[-\frac{1}{2}\nabla^2 - \frac{Z}{r}\right]\psi(r) = E\psi(r) \tag{3.2}$$

The quantity in square brackets means the kinetic and potential energy of an electron at a distance r from a nucleus of charge Z (1 for hydrogen). r is the electron coordinates. Wave functions for the hydrogen atom are the familiar s, p, d... atomic orbitals. The square of the wave function times a small volume results in the probability of finding the electron inside this volume (Hehre, 2003).

3.1.2. Hartree-Fock Approximation

Hartree-Fock assumes that each electron moves in an average potential field of all the other electrons in the system (Hehre, 2003). The Hartree Fock wavefunction, ϕ, which is a single determinant of n, one electron orbitals χ_i and the best set of χ_i are to be decided by the turning points in the Hartree-Fock Functional (Equation 3.3) (Cook, 2005).

$$E[\chi_i] = \frac{\int \phi * \widehat{H}\phi d\tau}{\int \phi * \phi d\tau} \tag{3.3}$$

3.1.3. Density Functional Models

Density functional theory is developed by Hohenberg and Kohn (1964), and Kohn and Sham (1965). Hohenborg and Kohn found out that the total energy of an electron gas is a unique functional of the electron density. The ground-state energy of the system is the minimum value of the total energy functional, and the density that generates this minimal value is the exact single-particle ground-state density (Payne *et al.*,1992). According to Kohn and Sham formula, the ground state energy, E is:

$$E = E_T + E_V + E_J + E_{XC} \tag{3.4}$$

where E_T is kinetic energy, E_V is the electron-nuclear interaction energy, E_J is Coulomb energy and E_{XC} is the exchange/correlation energy. Except for E_T all components depend on the total electron density, ρ(r):

$$\rho(r) = 2 \sum_{i}^{orbitals} |\psi_i(r)|^2 \tag{3.5}$$

where ψ_i are the Kohn-Sham orbitals and the summation is performed over pairs of electrons (Hehre, 2003).

E_{XC} is the only part that is not known exactly. Therefore, DFT model use different approximate expressions for E_{XC}. If it is assumed that E_{XC} is a local function of ρ, then local density approximation (LDA) is obtained. On the other hand, if E_{XC} depend on

derivatives of ρ, as well as ρ itself, generalized gradient approximation is attained (Yates and Johnson, 2007).

$$E_{XC}^{LDA}[\rho] = \int \rho(\vec{r})\varepsilon_{XC}^{LDA}[\rho(\vec{r})]\, d\vec{r} \tag{3.6}$$

$$E_{XC}^{GGA}[\rho] = \int \rho(\vec{r})\varepsilon_{XC}^{GGA}[\rho(\vec{r}), \nabla\rho(\vec{r}), \nabla^2\rho(\vec{r})]\, d\vec{r} \tag{3.7}$$

where $\varepsilon_{XC}(\rho)$ is the exchange-correlation energy per particle of homogenous electron gas density (Filippi *et al.*, 1996). Density Functional model is much more efficient than high-accuracy molecular orbital methods and gives results more accurate than Hartree-Fock approximation (Yates and Johnson, 2007).

3.1.4. Slab Models

An ideal model to study a surface can be developed from a piece of material that is infinite in two dimensions and finite along the surface normal. As seen on Figure 3.1 below, the supercell consists of atoms along fraction of the vertical direction. In the lower part of the supercell, the atoms occupy the entire supercell in the x and y directions, but in the top part of the supercell, the space has been left empty above the atoms. This model is named a slab model. The empty space disconnecting periodic images of slab along the z direction is named as vacuum space. There should be enough vacuum space between periodic slabs to minimize the effect between the slabs (Sholl and Steckel, 2009).

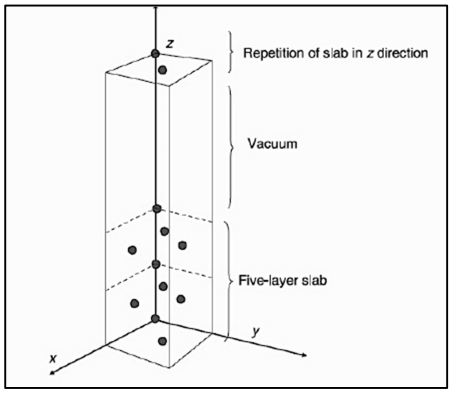

Figure 3.1. Schematic of a Supercell (Sholl and Steckel, 2009).

3.2. Materials Studio Software

3.2.1. Materials Studio (MS) Visualizer

DFT calculations were performed via Materials Studio (MS) 6.0 of Accelrys Inc while accomplishing this work. Models of molecules, crystalline materials, surfaces, polymers, and mesoscale structures can be built, maneuvered and monitored by MS Visualizer (Material Studio Overview, 2011).

In this study bulk crystal structure of Ni and Co metal is imported from MS database and optimized first. In Figure 3.2 bulk structure of Co and Ni are given.

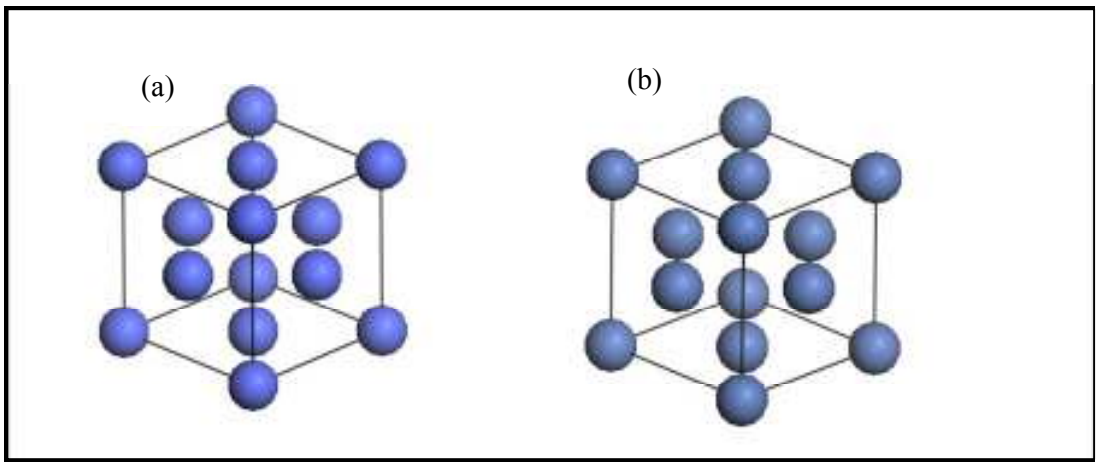

Figure 3.2. The Visual Models of (a) Co and (b) Ni Bulk Structure.

Secondly, slab structure of metal is constructed (Figure 3.3). Surface is cleaved by introducing Miller indices of surface and number of atomic layers. Then, vacuum is added along the z-direction to the slab, which is enough to guarantee ignoring any interaction between top and bottom of the following slab. In order to minimize computation time, slab thickness must be chosen deliberately. In general, surface layers of the slab kept relaxed while atoms at bottom layers are kept fixed in their bulk position to decrease computational cost.

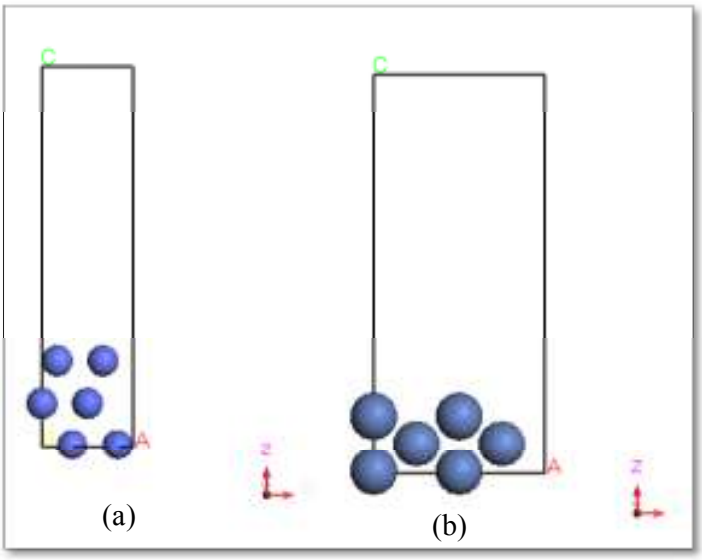

Figure 3.3. The Visual Models of (a) Co(111) and (b) Ni(220) Slab.

MS offers CASTEP and DMol^3 tools for energy calculations. Infinite separation of all electrons and nuclei refers to the zero energy, therefore the total energy of a molecule or a slab is generally negative.

3.2.2. MS DMol^3

Local density functional calculations or in short DMol^3 utilizes localized numerical orbitals as basis functions. DMol^3 depend on numerical integration in three dimensions for exchange and correlation matrix elements. A Harris functional form provides stability of the total energy and the atomic dissociation energy on approaching self-consistency (Delley 1990; Delley, 2000). DMol^3 can be applied on processes in gas phase, solution and solid environments. DMol^3 is capable for calculation of optimized geometry, transition state search and optimization, determination of reaction path, and frequency calculations (Materials Studio data sheet, 2011).

3.3. Calculational Parameters

Spin-polarized DFT calculations were performed with the program packages DMol^3 Materials Studio (version 6.0) of Accelrys Inc.

DFT calculations within the Local Density Analysis (LDA) and Perdew-Wang (PWC) functional with All Electron Relativistic (AER) core treatment and DNP basis set applied to investigate vibrational frequency of CH_x(x=0-4), CO_2, CO, and O on Co(111), Ni(220), and NiPt(220) which is constructed by replacing one Ni surface atom with one Pt atom. All calculations are carried out using DMol^3.

The slab is modeled as 3 layer slabs for all surfaces. For Co(111) slab, the uppermost two layers of the slab and the adsorbate were relaxed, and the remaining bottom layer were fixed in its bulk positions. For Ni (220) and NiPt (220) slab all three layers were fixed, while adsorbate is relaxed. The vacuum thickness between slabs was 14 Å to ensure no significant interaction between slabs.

In periodic DFT calculations, k-points sampling for Co (111) was 3x3x1 for 2x2 supercell and k-points sampling for Ni (220) and NiPt(220) was 3x4x1 for 2x2 supercell. A 4.3 Å global orbital cutoff and a Fermi smearing of 0.005 Hartree (Ha) were used. The convergence criteria for the structure optimization and frequency analysis were set to a SCF tolerance 1.0×10^{-5} Ha/atom, 2.0×10^{-5} Ha/atom for energy, 0.004 Ha/Å for maximum force and 0.005 Å for maximum displacement.

4. RESULTS AND DISCUSSION

The determination of the sites participating the reaction mechanism is of crucial importance in catalysis. Ni- and Co- based catalysts have been studied by our group for their activity in Catalytic Dry Reforming of Methane (CDRM). Although in-situ FTIR-DRIFT tests have been conducted on those catalysts under adsorption and reaction conditions, and the vibrational spectra were obtained, the available information in the literature is not detailed and surface specific enough to allow the determination of the active sites on the catalyst through comparative analysis with the FTIR-DRIFT data. The surface mechanisms of syngas (H_2+CO) production by dry reforming of methane (CDRM) involve simultaneous methane dehydrogenation and CO_2 dissociation. There the former produces hydrogen and surface carbon while the latter produces surface oxygen, which is used in cleaning carbon formed on dehydrogenation sites, and CO. The aim of this study is to form a vibrational frequency data base for CDRM reactants (CH_4 and CO_2), and intermediate species formed through CH_4 dehydrogenation, such as CH_3, CH_2, CH, C, and H, and CO and O formed through CO_2 dissociation on Co(111) flat surface, and Ni(220) and NiPt (220) terraced surfaces via using quantum mechanical (QM) codes utilizing Density Functional Theory (DFT). The frequency data set formed will be extremely valuable in finding the active sites of Ni and Co based CDRM catalysts through comparing calculated values with experimental in situ FTIR-DRIFT results.

Vibrational frequencies of molecules CH_4, CH_3, CH_2, CH, CO_2, CO and, C, H, and O atoms on Co(111), Ni (220) and NiPt(220) surfaces were investigated. The surfaces used in this study are the crystal faces formed on Co, Ni, and Pt-Ni catalysts that had been experimentally studied by our group. The presence of those crystal structures were confirmed by XRD analysis. The QM simulations were performed for all possible adsorption sites on these surfaces via using spin polarized DFT calculations with DMol^3 tool of Material Studio utilizing LDA-PWC functional.

4.1. Frequency Analysis of CH_x(x=0-4), H, CO_2, CO, and O on Co(1 1 1)

Frequency analysis was performed on 2x2 supercell with 1/4 MLE adsorbate molecule concentration. Prior to the simulations, adsorbates were placed 1.8 Å above the surface plane. The possible adsorption sites are shown on Figure 4.1. Calculated stretching frequencies for each molecule and atom on each adsorption site of Co (111) are listed in Table 4.1. Frequencies for CO_2 and CO molecules refer to vibration between C and O, for CH_x (x=4-1) molecule they refer to vibration between C and H, and for C, H, and O atoms they refer to vibration between atom and the coordinated metal.

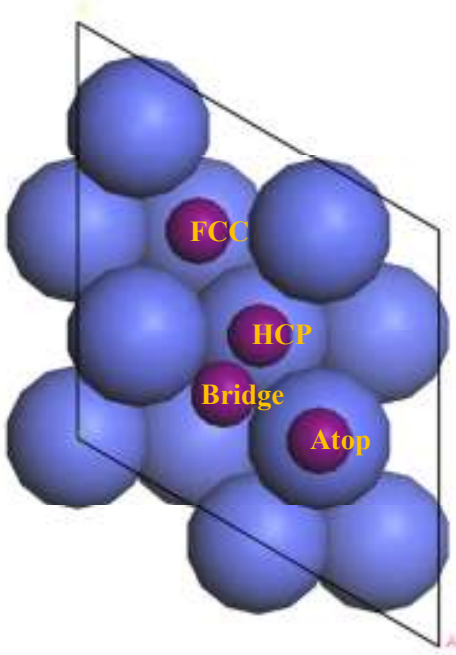

Figure 4.1. Top View of Co(111) Surface and All Possible Adsorption Sites. The Balls in Blue Color Represent Co Atom. Possible Adsorption Sites are Shown by Purple Balls and Labeled as Atop, Bridge, Face Centered Cubic (FCC) and Hexagonal Close Packed (HCP).

As given in Table 4.1, CO_2 has the highest vibrational frequency on the atop site of Co(111), which was found as 2205.08 cm^{-1}. Vasfiye Çimenoğlu (2011) also reported in her M.S. Thesis that, CO_2 has an endothermic adsorption energy on atop site of Co(111) and is not stable there. CO_2 placed on hcp and fcc sites moved to the bridge site and resulted in very close frequency values on the band between 2035-2047 cm^{-1}. On the other hand, as

mention in Section 2.6, CO_2 vibration was observed at 2360 and 2340 cm^{-1} band on Co/ MgO-SiO_2 catalyst (Bouarab *et al*., 2004). In another study, Yung *et al.* (2008) investigated surface species on CoO_x/ZrO_2 using DRIFTS and they obtained CO_2 frequency values between 2360 and 2335 cm^{-1}. Furthermore, Song *et al.* reported that bands around 2364 and 2338 cm^{-1} indicate the existence of gaseous CO_2 on Co/SiO_2 catalyst. As a general approach, various vibrational bands stem from the temperature and support type differences yielding differences in the active metal sites plays a role in reaction. Calculated stretching frequencies for CO_2 are, in general, consistent with the results of those experimental works.

Calculated CO frequencies on Co(111) at atop, bridge, HCP, and FCC sites, are 2078.49, 1878.92, 1773.99, and 1802.70 cm^{-1} (Table 4.1) respectively. While the highest frequency was acquired at atop site, the lowest frequency was obtained at HCP site. In general, adsorption energies and the vibrational frequencies are inversely related to each other. In accordance with the calculated values, the highest adsorption energies were found for HCP and FCC sites and the lowest one calculated for atop site of Co(111) (Çimenoğlu, 2011). In the literature, CO frequency is reported as between 2000 and 2200 cm^{-1} (Bouarab *et al.*, 2004; Mihaylova *et al.*, 2006; Song *et al.,*2007; Ulla *et al.*, 2001; Yung *et al.*, 2008). Specifically, Mihaylova obtained 2-frequency bands at 2208 and 2188 cm^{-1} on Co/AlBEA; the other frequencies for CO molecule attained on Co/SiBEA were 2185 and 2178 cm^{-1}. In another study, bands at 2170 and 2116 cm^{-1} conforms to CO frequency (Yung *et al.*, 2008). Furthermore, Song *et al.* (2007) described that the band around 1935 cm^{-1} corresponds to CO adsorbed on metal in bridge form, and the band around 2030 cm^{-1} refers to CO adsorbed on metal in linear/atop form. Although exactly the same values for CO stretching on Co(111) could not be calculated, frequencies found are considerably close the experimental results.

As shown in Table 4.1, O vibrational frequency on Co(111) was calculated around 552 cm^{-1} for atop and HCP sites, while it was calculated around 518 cm^{-1} for bridge and FCC sites. As O atom placed on atop site moved to the HCP site of Co(111), and that at bridge site moved to the FCC site of Co(111). This is the reason why at the end of geometry optimization, adjacent values are obtained; in Vasfiye Çimenoğlu's M.S. Thesis

(2011), equal O adsorption energies was detected on atop and HCP site, and the difference between the adsorption energies at bridge and FCC sites was infinitesimally small.

In the case of CH_4, the calculated C-H stretching frequencies are given in Table 4.1. Frequency of CH_4 molecule varies between 3685 and 3676 cm^{-1}. At all sites, stretching frequencies of CH_4 are very close to each other. As explained in Section 2.4.2 in a detailed fashion, Zuo *et al.* (2010) calculated the adsorption energy of CH_4 on Co(111) as very close to zero, and similar values for all possible adsorption sites indicate that interaction of CH_4 and Co(111) surface is very weak. Vasfiye Çimenoğlu (2011) also acquired similar results for CH_4 adsorption. During frequency analysis of CH_4 molecule in the current study, CH_4 molecule moved away from surface as in the work of Zuo *et al.* On the other hand, experimental FTIR-DRIFT works gave various but very similar frequency values for CH_4 molecule such as, 3018, 3015, and 3014 cm^{-1} (Yung *et al.*, 2007; Song *et al.*, 2007; Bouarab *et al.*, 2004). There is a gap between the experimental and the calculated values. As mention in the study of Zuo *et al.* (2010), this may be the result of lack of having right physics to account for van der Waals interactions in DFT calculations, thus DFT might not be a precise calculational method for such weak adsorptions.

Stretching frequency values for CH_3 molecule on Co(111) were calculated as 3141.73 cm^{-1} at FCC site, 3136.98 cm^{-1} at bridge site, 3605.93 cm^{-1} at atop site, and 3600.78 cm^{-1} at HCP site, as given in Table 4.1. CH_3 molecule, which is placed at HCP site, moves to atop site during geometry optimization and therefore CH_3 on these two sites has similar frequency values. Zuo *et al.* (2010) found the lowest CH_3 adsorption energy on Co(111) at atop site and the highest at HCP site, with 0.01 eV difference compared to that obtained for the FCC site. In this study, the highest frequency value was obtained for the adsorption at the atop site, and the lowest one acquired for the FCC site. Moreover, Zuo *et al.* (2010) reported that CH_3 positioned at bridge site is stabilized at HCP site on Co(111). In the literature, CH_3 molecule on Co metal was reported to have stretching frequency around 2968 cm^{-1} (Song *et al.*, 2007), which is in good agreement with the current study in case for FCC and bridge type CH_3 adsorptions.

CH_2 adsorption on Co(111) yields 3314.84 cm^{-1} frequency at atop site, 2930.67 cm^{-1} frequency at bridge site, 2975.33 cm^{-1} frequency at HCP site and 3113.47 cm^{-1} frequency

at FCC site (Table 4.1). C-H stretching frequency for CH_2 is the highest at atop site, conflicting with the results obtained by Zuo *et al*. who reported the lowest CH_2 adsorption energy calculated was for the adsorption at the atop site. C-H stretching frequency for CH_2 is the lowest at bridge site, however Zuo *et al.* calculated the highest adsorption energy belongs to the adsorption on HCP site. There it should be noted that CH_2 initially positioned at bridge site is stabilized there at the end of the optimization. Thus, inverse relation between vibrational frequency and adsorption energy of CH_2 molecule has been confirmed by the current results implicitly. Song *et al.*(2007) reported that bands at 2927 and 2864 cm^{-1} correspond to CH_2. The difference between experimental and calculated C-H stretching frequency values for HCP ($\Delta\nu$= 3.67 cm^{-1}) can be considered insignificant.

According to the study of Zuo *et al.* on Co(111), CH molecule has the lowest adsorption energy at atop site and the highest adsorption energy was obtained for CH at the HCP site. At atop site, CH molecule is closer to Co(111) surface compared with those for the other sites (Zuo *et al.*, 2010). As given in Table 4.1, CH atop adsorption on Co(111) yields the lowest C-H stretching frequency, which is 3004.85 cm^{-1}. The highest vibrational frequency of CH was calculated for adsorption at FCC site as 3185.32 cm^{-1}. At bridge site, C-H stretching frequency was calculated as 3113.11 cm^{-1}, while it is 3181.76 cm^{-1} for the HCP site.

Calculated vibrational frequencies between C and the metal surface are shown in Table 4.1. Frequency between C and coordinated metal atom(s) of Co(111) surface is 538.63 cm^{-1} at bridge site, while it is 525.19 cm^{-1} at FCC site. At atop site, C yielded the lowest frequency with 524.12 cm^{-1}, and in accordance with the current study, Zuo *et al.,* calculated the lowest adsorption energy for the atop site of Co(111) surface. After geometry optimization, C stabilizes at atop site closer to the upmost Co(111) surface, compared to the adsorbed C at the other sites. The highest vibrational frequency was obtained as 541.38 cm^{-1} at HCP site. Zuo *et al.* found out that C preferred to be adsorbed at HCP site, and C initially positioned at the bridge site diffuses to HCP site at the end of the geometry optimization. In the current study, bridge and HCP-adsorbed C give similar frequencies on Co(111) confirming the literature.

Table 4.1 also shows the computed vibrational frequency for the adsorbed H after optimization. As H originally positioned at atop site was stabilized at HCP site at the end of the optimization, H adsorption yielded very close stretching frequencies, 1004.25 and 1010.51 cm^{-1} at atop and HCP sites, respectively. Similarly, H at bridge and FCC sites, yielding very close frequency values 1028.96 cm^{-1} and 1021.89 cm^{-1}, respectively, as the H originally placed at bridge site moves to the FCC site at the end of the optimization. On the other hand, Zou *et al.* reported that H originally placed at bridge site diffused to HCP site after optimization, and H favored to be adsorbed at FCC site. After optimization, H placed atop comes more closer to upmost Co(111) surface, compared to that placed at the other sites (Zuo *et al.*, 2010).

For CH, C, and H, there is a linear relationship between the adsorption energies and vibrational frequencies on Co(111).

Table 4.1. Frequency of CO_2, CO, O, CH_4, CH_3, CH_2, CH, C and H at All Possible Adsorption Sites of 2x2 Supercell Co(111) Surface. Tabulated Adsorption Sites are The Original Sites before Geometry Optimization.

Adsorbed molecule	**Adsorption Site**	**Frequency (cm^{-1})**
CO_2	Atop	2205.08
CO_2	Bridge	2035.35
CO_2	HCP	2046.91
CO_2	FCC	2036.43
CO	Atop	2078.49
CO	Bridge	1878.92
CO	HCP	1773.99
CO	FCC	1802.70
O	Atop	552.15
O	Bridge	518.21
O	HCP	552.26
O	FCC	517.94
CH_4	Atop	3684.69
CH_4	Bridge	3676.77

Table 4.1. Frequency of CO_2, CO, O, CH_4, CH_3, CH_2, CH, C and H at All Possible Adsorption Sites of 2x2 Supercell Co(1 1 1) Surface. Tabulated Adsorption Sites are The Original Sites before Geometry Optimization (cont'd).

CH_4	HCP	3681.43
CH_4	FCC	3678.01
CH_3	Atop	3605.93
CH_3	Bridge	3136.98
CH_3	HCP	3600.78
CH_3	FCC	3141.73
CH_2	Atop	3314.84
CH_2	Bridge	2930.67
CH_2	HCP	2975.33
CH_2	FCC	3113.47
CH	Atop	3004.85
CH	Bridge	3113.11
CH	HCP	3181.76
CH	FCC	3185.32
C	Atop	524.12
C	Bridge	538.63
C	HCP	541.35
C	FCC	525.19
H	Atop	1004.25
H	Bridge	1028.96
H	HCP	1010.51
H	FCC	1021.89

4.2. Frequency Analysis of CH_x(x=0-4), H, CO_2, CO, and O on Ni(220)

The presence of Ni(111), Ni(200), and Ni(220) surfaces on Ni-Pt/δ-Al_2O_3 catalyst has been confirmed by XRD measurements (Çağlayan *et al.*, 2005; Selen, 2003). The flat Ni surface, Ni(111), and its interaction with CH_x and CO_x has been already studied by Merve Ayvaz (2013).

As the analysis of species involved in CDRM on terraced Ni surface is aimed in the current study, first frequency analysis of CH_x-Ni(220) system has been made and the results obtained are presented in Table 4.2. In the frequency analysis, 2x2 supercell with 1/4 MLE adsorbate molecule concentration was used. Adsorption sites i.e. atop, long-bridge (LB), short-bridge (SB), and fourfold hollow (FH), are shown in Figure 4.2. Calculated stretching frequencies for each molecule and atom on possible adsorption sites of Ni (220) are listed in Table 4.2. The reported stretching frequencies for CH_x are refer to vibration of molecular C-H bonds, frequencies for CO_2 and CO molecules refer to C-O molecular vibration, while for C, H, and O atoms they refer to vibration of adsorbate-coordinated metal atom bonds.

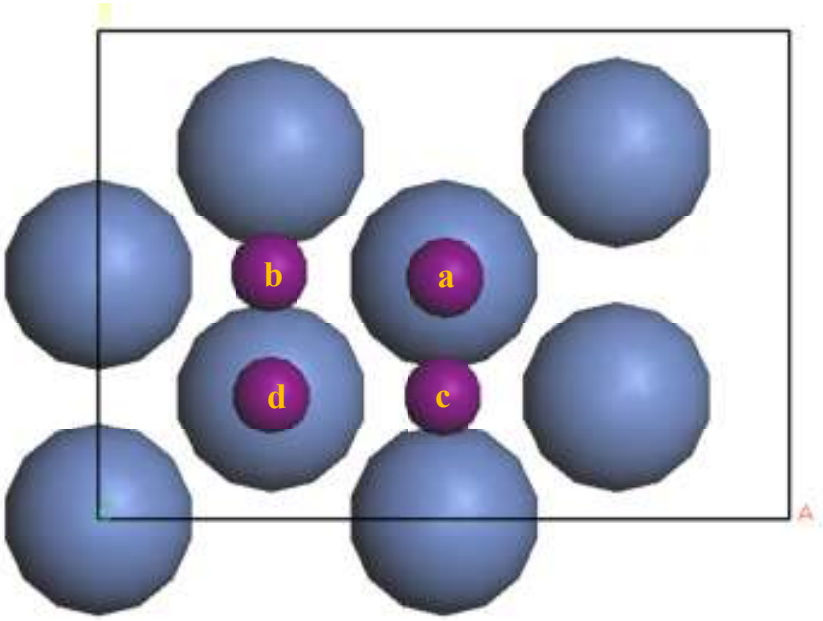

Figure 4.2. Top View of 2x2 Supercell Ni(220) Surface and All Possible Adsorption Sites. The Balls in Blue Color represent Ni Atom. Possible Adsorption Sites are Shown by Purple Balls and Labeled as (a) Atop, (b) Long-Bridge(LB), (c) Short-Bridge(SB), and (d) Fourfold Hollow (FH).

The computed vibrational frequency values of CH_4-Ni(220) system are given in Table 4.2. C-H stretching frequencies on Ni(220) are in the range 3678-3698 cm^{-1}. At all sites, CH_4 moves away from the surface indicating weak adsorption. CH_4 initially positioned atop stabilized at a site between atop and FH; similarly, SB-placed CH_4 was

stabilized at a site between SB and FH. In the literature, bands at 3016 cm^{-1} and 1305 cm^{-1} confirm the presence of gaseous CH_4 on Ni-ZrLa and Ni-Ca-ZrLa (Bachiller-Baeza *et al.*, 2013). In their study Bradford and Vannice (1996) assigned peaks at 3000 and 1300 to the CH_4 on Ni/SiO_2 and Ni/TiO_2. According to study of de Sousa *et al.* (2012), FTIR measurements performed on spent $Ni/NiAl_2O_4$ indicate C-H stretching band at 2935 cm^{-1}, and a broad band in the 3000-3470 cm^{-1} was proposed to be related to disordered carbon or C-H contributions. Calculated frequencies for CH_4 adsorption on Ni(220) in the current work are pretty higher than the experimental findings. The main reason behind the difference between experimental and calculated values is the fact that DFT miscalculate the weak adsorptions, which occur through Van der Waals interaction between the molecule and the surface without chemical bonding.

Vibrational frequencies obtained for CH_3 adsorbed on Ni(220) are presented in Table 4.2. CH_3 adsorbed on atop, LB and FH sites gave stretching frequencies in a short band between 3646-3669 cm^{-1}. Both LB and FH-placed CH_3 moved to atop position, which resulted in closer frequency values for those sites as 3669.11 and 3647.58 cm^{-1}, respectively, to the frequency obtained for atop coordination ca. 3646.83 cm^{-1}. CH_3 frequency at SB site on Ni (220) is 3449.32 cm^{-1}, which is remarkably different from those obtained for the other sites. On the other hand, band at 2860 cm^{-1} obtained from DRIFT spectra of CH_4 adsorption after flushing with Ar over Ni-ZrLa and Ni-Ca-ZrLa at 773 K is assigned to symmetric stretching vibrations of CH_3 (Bachiller-Baeza *et al.*, 2013). Computed frequencies for CH_3 adsorption on Ni(220) are extremely different from the proposed experimental vibration bands most probably due to geometry and/or support effect, and possible alloy formation as well, all of which, especially the latter, can change the electronic properties of the adsorption sites drastically.

CH_2 adsorbed on Ni(220) yields stretching frequency values in a wide range. On Ni(220), calculated stretching frequency values for CH_2 molecule were 3285.29 cm^{-1} at atop site, 2096.71 cm^{-1} at LB site, 3423.28 cm^{-1} at SB site, and 2843.59 cm^{-1} at FH site, as given in Table 4.2. While CH_2 bound at LB and FH were positioned extremely close to the surface, CH_2 bound at SB and atop site were moderately close to surface after geometry optimization. Furthermore, Bachiller-Baeza *et al.* (2013) reported that 2931 cm^{-1} band

refers to asymmetric CH_2 vibration. CH_2 frequency at fourfold hollow site in the current work is the closest one to this band with stretching frequency difference Δv=87.41 cm^{-1}.

Vibrational frequencies for CH adsorption on Ni(220) were calculated in the range 2735-2982 cm^{-1} (Table 4.2). The highest vibrational frequency was found for adsorption at SB site as 2982.34 cm^{-1}. Due to the tendency of CH to move to the SB site, a closer frequency value was obtained for the adsorption at FH site (ca. 2956.12 cm^{-1}). Lower frequencies were computed for atop and LB-coordinated CH on Ni(220) as 2867.06 and 2735.76 cm^{-1}, respectively.

As shown in Table 4.2, calculated vibrational frequencies of C are in the range 607-680 cm^{-1} except the one for FH site, 757.05 cm^{-1}, where C is greatly close to Ni(220) surface.

Table 4.2 also shows the computed vibrational frequency of the surface coordinated H after geometry optimization. H yielded vibrational frequency of 2010.85 cm^{-1} at atop site, which is the highest vibrational frequency on Ni(220) bounded H. H adsorbed on LB presents the lowest vibrational frequency as 962.49 cm^{-1}. Initially FH-placed H has a tendency to move to SB site after optimization; therefore, H adsorbed at SB and FH resulted in close frequency values calculated, ca. 1203.26 cm^{-1} and 1198.26 cm^{-1}, respectively. H bound at LB, SB, and FH are intensely close to the surface, whereas H placed at atop site is moderately close to the surface.

CO_2 vibrational frequencies on possible adsorption sites of Ni(220) were obtained in the range of 1996.67-2353 cm^{-1} (Table 4.2). The highest vibrational frequency for CO_2 was calculated as 2353.24 cm^{-1} for the adsorption at atop site. Short-bridge (SB) CO_2 adsorption yields 2081.57 cm^{-1} frequency, while CO_2 adsorption at long-bridge (LB) yields 2062.95 cm^{-1} frequency. The difference between CO_2 stretching frequency values for the adsorption at SB to LB sites 18.62 cm^{-1}, is very small. For fourfold (FH) type adsorption, the stretching frequency was computed as 1996.67 cm^{-1}, which is the lowest stretching CO_2 frequency calculated on Ni(220). In the literature, CO_2 vibrational band is reported around 2300 cm^{-1}. (Bachiller-Baeza *et al.,* 2013; Ni *et al*., 2012; Bradford and Vannice, 1996). As mention in Section 2.6 in a detailed fashion, Bachiller-Baeza *et al.* reported CO_2

rotation-vibration frequency as 2360 and 2340 cm^{-1}, while Ni *et al.* measured adsorbed CO_2 has a vibrational frequency of 2328 cm^{-1} on Ni/B_2O_3-Al_2O_3, and Bradford and Vannice obtained 2300 cm^{-1} frequency for CO_2 on Ni/SiO_2. Thus, calculations performed for CO_2 atop adsorption on Ni(220) yielded the most consistent vibrational frequency values considering those experimental findings.

As CO originally placed at LB position moved to the atop position after geometry optimization, CO adsorption at atop and LB sites of Ni (220) yielded C-O stretching frequencies very close to each other, i.e. 2130.64 cm^{-1} and 2128.07 cm^{-1} (Table 4.2). At SB site of Ni(220), CO vibrational frequency (2021.42 cm^{-1}) is lower than those obtained for adsorption at LB and atop sites. Furthermore, the lowest frequency was calculated as 1813.69 cm^{-1} for CO adsorbed at FH site of Ni(220). CO is a probe molecule for DRIFT studies; therefore, there is a broad literature reporting stretching frequency values of the adsorbed CO molecule. Two vibrational peaks, at 2181 and 2121 cm^{-1}, were obtained for CO adsorbed CDRM catalysts, Ni-Ca-ZrLA and Ni-ZrLa (Bachiller-Baeza *et al.*, 2013). During CDRM reaction on the Ni/SiO_2 surface, both linear (ca. 2050 cm^{-1}) and bridged (ca. 1935 cm^{-1}) forms of CO were identified (Bradford and Vannice, 1996). In the characterization of alumina supported Pt, Ni and PtNi alloy catalysts, Garcia-Dieguez *et al.* reported that the band at 2167-2173 cm^{-1} is assigned to CO interacting with Ni^{2+} ions, and they also proposed that bands lower than 2000 cm^{-1} indicate bridge and triple bridge bonded CO. Linearly adsorbed CO on Ni yields stretching frequencies between 2100 and 2000 cm^{-1} while the bridged CO yields frequency values below 2000 cm^{-1}(Pompeo *et al*., 2007). Furthermore, in Ph.D. Thesis of Feyza Gökaliler, CO bands were detected at 2057, 2038 and 2007 cm^{-1} corresponding linearly adsorbed CO on Ni^0, the bands at 1938 and 1860 cm^{-1} are assigned to bridged CO on Ni (111) and Ni(100). All frequency data for all possible sites of Ni(220) calculated in the current study are in good agreement with the literature. Results of the current study show that originally CO positioned at atop, LB and SB assumed its original form, without any inclination to the surface plane, at the end of simulations, for which the vibrational frequency is calculated above 2000 cm^{-1}. On the other hand, CO has begun to change its spatial orientation and became inclined to the surface plane at FH site, where CO stretching frequency was computed below 2000 cm^{-1}.

Table 4.2 also shows the computed vibrational frequency of O on Ni(220). Calculated O frequencies on Ni(220) are 753.17, 449.96, 670.57 and 561.82 cm^{-1} at atop, LB, SB, and FH sites, respectively. The highest frequency obtained from O-Ni(220) system is for O at atop site, while the lowest one obtained for adsorption at LB site. FH-positioned O atom leaves its initial position and stays between SB and FH at the end of the geometry optimization; this is the reason why O frequency at FH site is closer to that at SB.

Table 4.2. Frequency of CO_2, CO, O, CH_4, CH_3, CH_2, CH, C and H at all Possible Adsorption Sites of 2x2 Supercell Ni(220) Surface. Tabulated Adsorption Sites are The Original Sites before Geometry Optimization.

Adsorbed molecule	**Adsorption Site**	**Frequency (cm^{-1})**
CH_4	Atop	3678.58
CH_4	LB	3686.83
CH_4	SB	3698.60
CH_4	FH	3682.75
CH_3	Atop	3646.83
CH_3	LB	3669.11
CH_3	SB	3449.32
CH_3	FH	3647.58
CH_2	Atop	3285.29
CH_2	LB	2096.71
CH_2	SB	3423.28
CH_2	FH	2483.59
CH	Atop	2867.06
CH	LB	2735.76
CH	SB	2982.34
CH	FH	2956.12
C	Atop	607.65
C	LB	636.52
C	SB	680.50
C	FH	757.05

Table 4.2. Frequency of CO_2, CO, O, CH_4, CH_3, CH_2, CH, C and H at All Possible Adsorption Sites of 2x2 Supercell Ni(220) Surface. Tabulated Adsorption Sites are The Original Sites before Geometry Optimization (cont'd).

H	Atop	2010.85
H	LB	962.49
H	SB	1203.26
H	FH	1198.26
CO_2	Atop	2353.24
CO_2	LB	2062.95
CO_2	SB	2081.57
CO_2	FH	1996.67
CO	Atop	2130.64
CO	LB	2128.07
CO	SB	2021.42
CO	FH	1813.69
O	Atop	753.17
O	LB	449.96
O	SB	670.57
O	FH	561.82

4.3. Frequency Analysis of CH_x(x=0-4), H, CO_2, CO, and O on NiPt(220)

Frequency analysis was performed on (220) face of NiPt alloy having Pt concentration 0.25. It should be noted that those atoms labeled with "1" in Figure 4.3 form the upmost layer. In the simulations, 2x2 supercell with 1/4 MLE adsorbate molecule concentration was used. Possible adsorption sites on NiPt(220) are shown in Figure 4.3. Calculated stretching frequencies for each molecule and atom adsorbed at the sites of NiPt(220) are listed in Table 4.3 and Table 4.4. As in the case of other surfaces analyzed in this work, calculated vibrational frequencies for CO_2 and CO molecules refer to vibration of C-O molecular bond, for CH_x (x=4-1) molecule they refer to vibration of C-H molecular bond, while for C, H, and O atoms they refer to vibration of adsorbate-metal bond.

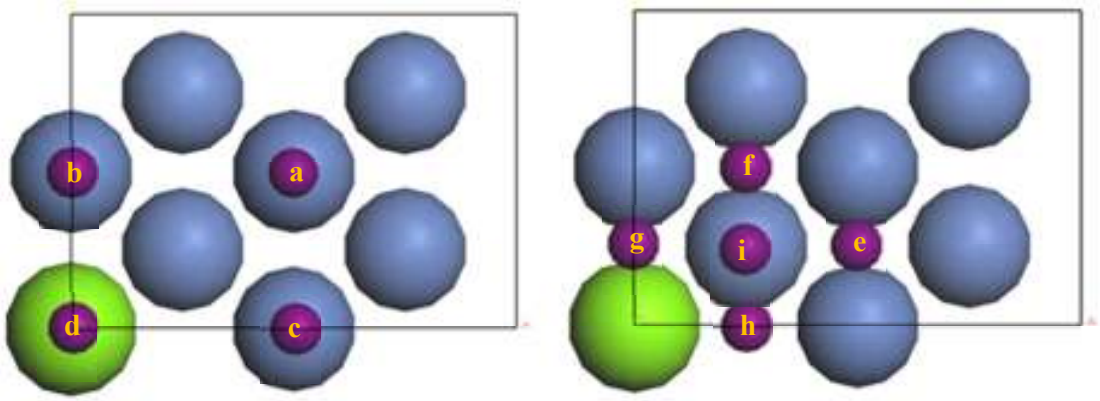

Figure 4.3. Top View of 2x2 Supercell NiPt(220) Surface and all Possible Adsorption Sites. The Balls in Blue Color Represent Ni Atom, in Green Color represent Pt Atom. Possible Adsorption Sites are Shown by Purple Balls and Labeled as (a) Atop Ni, (b) Atop Ni-close, (c) Atop Ni-far, (d) Atop Pt, (e) Ni-Ni Short-bridge (SB), (f) Ni-Ni Long-bridge (LB), (g) Ni-Pt Short-bridge (SB), (h) Ni-Pt Long-bridge (LB), and (i) Fourfold hollow (FH).

Vibrational frequencies for CO_2, CO, and O on NiPt(220) are summarized in Table 4.3. In general, Pt existence affects the vibrational frequency of CO_2 on NiPt(220). For atop coordinated adsorption systems, CO_2 frequencies are around 2340 cm^{-1} for atop Ni, atop Ni-far, for which CO_2 is positioned far from Pt atom at the supercell, and atop Pt sites. At atop Ni-close, which is close to Pt atom at the supercell, yielded lower frequency (ca. 2294.55 cm^{-1}) values than those obtained for adsorption on other atop sites. CO_2 vibrational frequencies were calculated as 2173.64 cm^{-1} at Ni-Ni SB where both legs are bound to Ni atoms. At Ni-Pt SB site, where one leg is at Pt and the other leg is at Ni, CO_2 vibrational frequency increased to 2207.27 cm^{-1}. CO_2 adsorption at Ni-Ni LB yielded stretching frequency of 2328.32 cm^{-1}, while at Ni-Pt LB, a lower frequency 2311.64 cm^{-1} was obtained. Pt presence increases the CO_2 frequency at SB, whereas decreases the CO_2 frequency at LB. The lowest CO_2 frequency obtained for CO_2 adsorbed at NiPt(220) sites was found as 2167.51 cm^{-1} for FH site. Wang *et al.* (2014) reported that the band at 2358 cm^{-1} indicates the C=O stretching on NiPt. CO_2 vibrational frequencies calculated in the current study for atop positions on Ni(220) are the closest values to this experimental finding.

CO adsorption at atop Ni and atop Ni-far yielded stretching frequencies as 2112.96 cm^{-1} and 2116.15 cm^{-1}, respectively. CO originally positioned at Pt-atop move to atop Ni-close and yielded frequencies around 2105 cm^{-1}. CO stretching frequency was found around 1962 cm^{-1} for both Ni-Pt SB and Ni-Pt LB sites, indicating the Pt presence show the same effect for both bridge sites. For CO coordinated at Ni-Ni SB position, a higher C-O frequency was obtained as 1993.87 cm^{-1}. CO initially positioned at Ni-Ni LB and FH sites moved to atop Ni-close site after geometry optimization yielding very close frequencies, 2106.26 cm^{-1} and 2105.18 cm^{-1}, respectively. In the literature, C≡O stretching frequency is detected at 2170 cm^{-1} (Wang *et al.*, 2014). According to DRIFT measurements, the band at ca. 2176 cm^{-1} is assigned to Ni^{2+}–CO. The very labile component at ca. 2156 cm^{-1} can be due to CO interacting with surface hydroxyl groups, and/or to Pt^{2+}–CO species on 0.04Pt4Ni/Al_2O_3. On the other hand, the bands at 2089–2060 cm^{-1} and 1938–1925 cm^{-1} resemble to CO adsorbed on Pt(100) surface. The three bands at 2067, 2037 and 2012 cm^{-1} are assigned to Ni^0 polycarbonyls, like $Ni(CO)_3$. (Garcia-Dieguez *et al.*, 2010). According to Feyza Gökaliler's PhD. Thesis, bands assigned to linear (2057 and 2038 cm-1) and bridge (1936, 1872, 1851 and 1843 cm-1) coordinated CO adsorption on monometallic nickel catalyst were also found at very close and intense wavelengths on bimetallic Pt-Ni catalyst. All calculated CO vibrational frequencies in the current work are consistent with the literature.

O vibrational frequencies on NiPt(220) were calculated in the range 736-788 cm^{-1} for atop Ni, atop Ni-close, atop Ni-far, Ni-Pt SB, and FH sites. O positioned at both FH and atop Ni-close sites diffused to Ni-Pt SB site and gave the adjacent values to that obtained for O at Ni-Pt SB, ca. 763.17 cm^{-1}. The highest O vibrational frequency was obtained as 953.64 cm^{-1} for O adsorbed at atop Pt site. O adsorption on Ni(220) yielded vibrational frequencies as 603.27, 333.66 and 276.34 cm^{-1} at Ni-Ni SB, Ni-Ni LB and Ni-Pt LB sites, respectively.

Table 4.3. Frequency of CO_2, CO, and O at All Possible Adsorption Sites of 2x2 Supercell NiPt(220) Surface. Tabulated Adsorption Sites are The Original Sites before Geometry Optimization.

Adsorbed molecule	**Adsorption Site**	**Frequency (cm^{-1})**
CO_2	Atop Ni	2340.51
CO_2	Atop Ni-close	2294.55
CO_2	Atop Ni-far	2341.43
CO_2	Atop Pt	2340.51
CO_2	Ni-Ni SB	2173.64
CO_2	Ni-Ni LB	2328.32
CO_2	Ni-Pt SB	2207.27
CO_2	Ni-Pt LB	2311.64
CO_2	FH	2167.51
CO	Atop Ni	2112.96
CO	Atop Ni-close	2105.74
CO	Atop Ni-far	2116.15
CO	Atop Pt	2106.23
CO	Ni-Ni SB	1993.87
CO	Ni-Ni LB	2106.26
CO	Ni-Pt SB	1962.84
CO	Ni-Pt LB	1962.49
CO	FH	2105.18
O	Atop Ni	788.09
O	Atop Ni-close	762.92
O	Atop Ni-far	782.66
O	Atop Pt	953.94
O	Ni-Ni SB	603.27
O	Ni-Ni LB	333.66
O	Ni-Pt SB	763.17
O	Ni-Pt LB	276.34
O	FH	736.63

As shown in Table 4.4, CH_4 adsorption on NiPt(220) gave C-H stretching frequencies in the range of 3678-3692 cm^{-1}. CH_4 adsorbed at atop Ni and atop Ni-far sites yielded frequency values around 3685 cm^{-1}. The highest C-H stretching frequency obtained is for CH_4 adsorbed at atop Pt as 3692.00 cm^{-1}. At atop Ni-close site, CH_4 vibrational frequency was computed as 3690.07 cm^{-1}, indicating that the presence of Pt led to a similar but higher frequency. CH_4 initially positioned at the bridge type-sites, i.e. at Ni-Ni LB and Ni-Pt SB was stabilized at atop Ni-close position yielding CH_4 vibrational frequency around 3688 cm^{-1}. Furthermore, CH_4 vibrational frequency is the lowest and calculated around 3678 cm^{-1} for methane coordinated at FH and Ni-Pt LB sites. In the literature, Wang *et al.* assigned the band at 3016 cm^{-1} to C-H stretching frequency. Our calculated CH_4 stretching frequency values are different from those values reported in experimental studies in the literature, most probably due to weak CH_4 adsorption on NiPt, which cannot be precisely simulated by DFT.

As shown in Table 4.4, vibrational frequency of CH_3 at atop Pt position of NiPt(220) was calculated as 3709.42 cm^{-1}. For atop Ni-far and atop-Ni positions lower CH_3 vibrational frequencies were calculated as 3704.58 and 3703.95 cm^{-1}, respectively. Furthermore, C-H stretching frequency decreases to 3675.89 cm^{-1} for CH_3 adsorbed at atop Ni-close site. Among the other bridge positions the lowest frequency was acquired as 3543.43 cm^{-1} at Ni-Ni SB site, CH_3 molecule originally positioned at Ni-Ni LB, Ni-Pt SB, and FH moved to atop Ni-close yielding frequencies as 3692.75, 3663.73, and 3680.97 cm^{-1}, respectively. CH_3 positioned originally at Ni-Pt LB site stabilized at Pt atop and yielded the highest vibrational frequency as 3713.84 cm^{-1}.

Calculated vibrational frequencies of CH_2 on NiPt(220) are given in Table 4.4. CH_2 adsorption at atop Ni-far yielded the highest vibrational frequency as 3700.06 cm^{-1}. Stretching frequency calculated for CH_2 adsorption at atop Ni position, 3694.29 cm^{-1}, is relatively lower. Both atop Pt and atop Ni-close placed CH_2 diffused to Ni-Pt SB site and yield much lower frequencies as 3584.98 and 3602.66 cm^{-1}, respectively. On the other hand, both Ni-Pt LB and Ni-Ni LB placed CH_2 have a tendency to move Ni-Pt SB site and gave extremely close frequencies to that computed for adsorption at Ni-Pt SB as 3598.71 cm^{-1}. At Ni-Ni SB, vibrational frequency of adsorbed CH_2 was calculated as 3680.35 cm^{-1}. Vibrational frequency of CH_2 adsorbed at FH site is 3598.16 cm^{-1} and it is very close to

value that obtained for CH_2 at Ni-Pt SB site, which is resulted from the fact that FH-placed CH_2 moves to Ni-Pt SB site after geometry optimization.

Calculated vibrational frequencies obtained for the CH-NiPt(220) system are given in Table 4.4. For CH adsorbed atop Ni and atop Ni-close, the calculated vibrational frequency is around 2979 cm^{-1}. While vibrational frequency slightly decreases to 2970.66 cm^{-1} for CH adsorbed at atop Ni-far site, it increases to 3202.64 cm^{-1} for CH adsorbed at atop Pt site. The highest CH vibrational frequency was determined for Ni-Pt SB site as 3218.74 cm^{-1}. CH adsorption at Ni-Ni SB yielded C-H frequency of 3198.05 cm^{-1}, whereas frequency declines to 3030.80 for CH adsorbed at Ni-Ni LB. The lowest vibrational frequency of CH on NiPt(220) was acquired at Ni-Pt LB site as 2782.21 cm^{-1}. CH adsorbed on both Ni-Ni LB and Ni-Pt LB sites is extremely close to upmost surface plane, therefore they yields relatively lower frequencies compared to that calculated for CH at other bridge type sites. The results show that Pt addition leads to an increase in vibrational frequency of CH at SB type-sites but, on the contrary, it decreases C-H vibrational frequency for LB type-sites. CH vibrational frequency was computed as 3137.48 cm^{-1} for CH adsorption at FH site.

As shown in Table 4.4, C adsorbed on possible NiPt(220) sites yielded very distinct C-metal frequencies. At atop Pt, Pt-C vibrational frequency was calculated as 685.77 cm^{-1}, and it increases to 706.62 cm^{-1} for C at atop Ni, and to 724.83 and 727.09 cm^{-1} for C at atop Ni-close and atop Ni-far sites, respectively. Among the C coordinated bridge sites, the lowest C-metal frequency was obtained for Ni-Pt LB as 518.17 cm^{-1}, while it shifts to 606.17 cm^{-1} for C at Ni-Ni LB, demonsrating that existence of Pt decreases the C-metal frequency at LB. C adsorption at Ni-Ni SB yielded frequency as 716.88 cm^{-1}, and the vibrational frequency value increases to 788.52 cm^{-1} when one of the Ni at the legs of the bridge is replaced by Pt. FH-placed C left its initial position and moved to the Ni-Pt LB site yielding very close C-metal frequency as ca. 520.26 cm^{-1}.

Vibrational frequencies of atop bound H were calculated in the range 2025-2111 cm^{-1} (Table 4.4). Pt addition lowers the H-metal frequency on NiPt(220) for atop type adsorption. The highest vibrational frequency was calculated for H adsorbed at atop Ni-far site as 2111.19 cm^{-1}, and it declines to 2105.74 cm^{-1} for H at atop Ni site. H placed at atop

Pt diffused the atop Ni-close site; consequently the H-metal vibrational frequency values calculated upon geometry optimization, 2038.21 cm^{-1} and 2025.38 cm^{-1} for atop H adsorbed Ni-close and atop Pt, respectively, are very close to each other. For bridge type H adsorption, Pt has an increasing effect on H-metal frequency for SB, whereas a decreasing effect for LB type adsorptions. H adsorbed at Ni-Ni SB yielded vibrational frequency of 1242.36 cm^{-1} and that at Ni-Pt SB the frequency increases to 2042.53 cm^{-1}. As H originally placed at Ni-Pt SB stabilized at atop Ni-close site; the frequency obtained for the atop Ni-close site is similar to that calculated for Ni-Pt SB site. At Ni-Ni LB, H-metal frequency was obtained as 912.37 cm^{-1}, and decreases to 726.36 cm^{-1} for at Ni-Pt LB site. FH placed H has a tendency to stabilize at Ni-Ni SB site yielding H-metal frequency of 992.18 cm^{-1}.

Table 4.4. Frequency of CH_4, CH_3, CH_2, CH, C and H at All Possible Adsorption Sites of 2x2 Supercell NiPt(220) Surface. Tabulated Adsorption Sites are The Original Sites before Geometry Optimization.

Adsorbed molecule	**Adsorption Site**	**Frequency (cm^{-1})**	**Adsorbed molecule**	**Adsorption Site**	**Frequency (cm^{-1})**
CH_4	Atop Ni	3685.24	CH_3	Atop Ni	3703.95
CH_4	Atop Ni-close	3690.07	CH_3	Atop Ni-close	3675.89
CH_4	Atop Ni-far	3685.15	CH_3	Atop Ni-far	3704.58
CH_4	Atop Pt	3692.00	CH_3	Atop Pt	3709.42
CH_4	Ni-Ni SB	3686.89	CH_3	Ni-Ni SB	3543.43
CH_4	Ni-Ni LB	3688.22	CH_3	Ni-Ni LB	3692.75
CH_4	Ni-Pt SB	3688.86	CH_3	Ni-Pt SB	3663.73
CH_4	Ni-Pt LB	3678.56	CH_3	Ni-Pt LB	3713.84
CH_4	FH	3678.45	CH_3	FH	3680.97
CH_2	Atop Ni	3694.29	CH	Atop Ni	2979.49
CH_2	Atop Ni-close	3602.66	CH	Atop Ni-close	2979.24
CH_2	Atop Ni-far	3700.06	CH	Atop Ni-far	2970.66
CH_2	Atop Pt	3584.98	CH	Atop Pt	3202.64
CH_2	Ni-Ni SB	3680.35	CH	Ni-Ni SB	3198.05
CH_2	Ni-Ni LB	3598.77	CH	Ni-Ni LB	3030.80
CH_2	Ni-Pt SB	3598.71	CH	Ni-Pt SB	3218.74

Table 4.4. Frequency of CH_4, CH_3, CH_2, CH, C and H at All Possible Adsorption Sites of 2x2 Supercell NiPt(220) Surface. Tabulated Adsorption Sites are The Original Sites before Geometry Optimization (cont'd).

Adsorbed molecule	**Adsorption Site**	**Frequency (cm^{-1})**	**Adsorbed molecule**	**Adsorption Site**	**Frequency (cm^{-1})**
CH_2	Ni-Pt LB	3598.64	CH	Ni-Pt LB	2782.21
CH_2	FH	3598.16	CH	FH	3137.48
C	Atop Ni	706.62	H	Atop Ni	2105.74
C	Atop Ni-close	724.83	H	Atop Ni-close	2038.21
C	Atop Ni-far	727.09	H	Atop Ni-far	2111.19
C	Atop Pt	685.77	H	Atop Pt	2025.28
C	Ni-Ni SB	716.88	H	Ni-Ni SB	1242.36
C	Ni-Ni LB	606.17	H	Ni-Ni LB	912.37
C	Ni-Pt SB	788.52	H	Ni-Pt SB	2042.53
C	Ni-Pt LB	518.17	H	Ni-Pt LB	726.36
C	FH	520.26	H	FH	992.18

5. CONCLUSIONS AND RECOMMENDATIONS

5.1. Conclusions

The current study aims to obtain vibrational frequency database for reactants, products, and intermediate species of CDRM on Co(111), Ni(220) and NiPt(220) surfaces through using DFT calculations.

Vibrational frequency of CH_4 is inconsistent with the literature for all surfaces; this may be the result of lack of having right physics to account for van der Waals interactions in DFT calculations, thus DFT might not be a precise calculational method for such weak adsorptions.

Calculated stretching frequencies for CO_2, CO, CH_3, and CH_2 on Co(111) are, in general, consistent with the results of those experimental works.

Adsorption energies of CO_2, CO, O, CH_4, CH_3, and CH_2 on Co(111) are inversely related with their stretching frequencies whereas there is a linear relationship for CH, C, and H on Co(111).

Calculated vibrational frequencies of CO_2, CO, and CH_2 on Ni(220) are consistent with the literature, while computed stretching frequencies for CH_3 on Ni(220) are extremely different from the proposed experimental vibration bands; most probably due to geometry and/or support effect, and possible alloy formation as well, all of which, especially the latter, can change the electronic properties of the adsorption sites drastically.

In general, Pt existence affects the vibrational frequencies of all species on NiPt(220) considering monometallic Ni(220) surface. Moreover, CO_2 and CO vibrational frequencies on NiPt(220) are considerably close to experimental findings.

The results show that Pt addition leads to an increase in vibrational frequencies of CH, C, and H at SB type-sites but on the contrary, it decreases vibrational frequencies of those species at LB type-sites.

5.2. Recommendations

The adsorption/co-adsorption behavior of reactants, intermediates and products species of CDRM should be studied on Ni(220) and NiPt(220), in order to obtain a relation between vibrational frequency values and adsorption energies of these species.

Other surfaces of Co and Ni that are obtained from XRD analysis should be studied in terms of vibrational frequencies of CDRM species.

Co-adsorbed CH_4 and CO_2 vibrational frequency should be calculated to compare FTIR-DRIFT results that obtained during CDRM reaction more realistically.

REFERENCES

Akpan, E., Y. Sun, P. Kumar, H. Ibrahim, A. Aboudheir, and R. Idem, 2007, "Kinetics, Experimental and Reactor Modeling Studies of the Carbon Dioxide Reforming of Methane (CDRM) over a New Ni/CeO2–ZrO2 Catalyst in A Packed Bed Tubular Reactor", *Chemical Engineering Science*, Vol. 62, pp. 4012-4024.

Ayvaz, M., 2013, *The Theoretical Analysis of The Interaction between Methane Dehydrogenation and Carbon Dioxide Dissociation Products with Ni and PtNi Surfaces*, M.S. Thesis, Boğaziçi University.

Bachiller-Baezaa, B., C. Mateos-Pedrero, M.A. Soria, A. Guerrero-Ruiz, U. Rodemerck, I. Rodríguez-Ramos, 2013, "Transient studies of low-temperature dry reforming of methane over Ni-CaO/ZrO_2-La_2O_3", *Applied Catalysis B:Environmental,* Vol. 129, pp. 450-459.

Barama, S., C. Dupeyrat-Batiot, M. Capron, E. Bordes-Richard, and O. Bakhti-Mohammedi, 2009, "Catalytic Properties of Rh, Ni, Pd and Ce Supported on Al-Pillared Montmorillonites in Dry Reforming of Methane", *Catalysis Today*, Vol.141, pp. 385-392.

Bouarab, R., O. Akdim, A. Auroux, O. Cherifi, and C. Mirodatos, 2004, "Effect of MgO Additive on Catalytic Properties of Co/SiO_2 in the Dry Reforming of Methane", *Applied Catalysis A: General*, Vol. 264, pp. 161-168.

Bouarab, R., O. Cherifi, and A. Auroux, 2005, "Effect of the Basicity Created by La_2O_3 Addition on the Catalytic Properties of Co(O)/SiO_2 in CH_4+CO_2 Reaction", *Thermochimica Acta*, Vol. 434, pp. 69-73.

Bradford, M. C. J. and M. A. Vannice, 1996, "Catalytic Reforming of Methane with Carbon Dioxide over Nickel Catalysts II. Reaction Kinetics", *Applied Catalysis A: General,* Vol. 142, pp. 97-122.

Bradford, M. C. J. and M. A. Vannice, 1999, "CO_2 Reforming of CH_4", *Catalysis Reviews: Science and Engineering*, Vol.41, No.1, pp. 1-42.

Carvalho, D. C., H. S. A. de Souza, J. M. Filho, A. C. Oliveira, A. Campos, É. R.C. Milet, F. F. de Sousa, E. Padron-Hernandez, and A. C. Oliveira, 2014, "A Study on the Modification of Mesoporous Mixed Oxides Supports for Dry Reforming of Methane by Pt or Ru", *Applied Catalysis A: General*, Vol. 473, pp. 132-145.

Cook, D. B., 2005, *Handbook of Computational Quantum Chemistry*, Dover Publications Inc., USA.

Çağlayan, B.S., A. K. Avcı, Z. İ. Önsan, and A. E. Aksoylu, 2005, "Production of Hydrogen over Bimetallic Pt–Ni/δ-Al_2O_3 I. Indirect Partial Oxidation of Propane", *Applied Catalysis A: General,* Vol. 280, pp. 181-188.

Çimenoğlu, V., 2011, *A Theoretical Study on Dry Reforming of Methane (CDRM) over Cobalt Metal*, M.S. Thesis, Boğaziçi University.

Dal Santo, V., A. Gallo, A. Naldoni, M. Guidotti, and R. Psaro, 2012, "Bimetallic Heterogeneous Catalysts for Hydrogen Production", *Catalysis Today*, Vol. 197, pp. 190-205.

Damyanova, S., B. Pawelec, K. Arishtirova, J. L. G. Fierro, C. Sener, and T. Dogu, 2009, "MCM-41 Supported PdNi Catalysts for Dry Reforming of Methane", *Applied Catalysis B:Environmental,* Vol. 92, pp. 250-261.

de la Peña O'Shea, V. A., S. González, F. Illas, and J.L.G. Fierro, 2008, "Evidence for Spontaneous CO_2 Activation on Cobalt Surfaces", *Chemical Physical Letters*, Vol. 454, pp. 262-268.

de Sousa, F. F., H. S. A. de Sousa, A. C. Oliveira, A. C. Oliveira, M.C.C. Junior, A. P. Ayala, E. B. Barros, B. C. Viana, J. M. Filho, and A. C. Oliveira, 2012, "Nanostructured Ni-Containing Spinel Oxides for the Dry Reforming of Methane:

Effect of the Presence of Cobalt and Nickel on the Deactivation Behaviour of Catalysts", *International Journal of Hydrogen Energy*, Vol. 37, pp. 3201-3212.

de Sousa, H. S. A., A. N. da Silva, A. J. R. Castro, A. Campos, J. M. Filho, and A. C. Oliveira, 2012, "Mesoporous Catalysts for Dry Reforming of Methane: Correlation between Structure and Deactivation Behaviour of Ni-containing Catalysts", *International Journal of Hydrogen Energy*, Vol. 37, pp. 12281-12291.

Delley, B., 1990, "An Allelectron Numerical Method for Solving the Local Density Functional for Polyatomic Molecules", *The Journal of Chemical Physics*, Vol. 92, pp. 508-517.

Delley, B., 2000, "From Molecules to Solids with the $Dmol^3$ Approach", *The Journal of Chemical Physics*, Vol. 113, No.18, pp. 7756-7764.

Djinović, P., J. Batista, and A. Pintar, 2012, "Efficient Catalytic Abatement of Greenhouse Gases: Methane Reforming with CO_2 Using A Novel and Thermally Stable Rh-CeO_2 Catalyst", *International Journal of Hydrogen Energy*, Vol. 37, pp. 2699-2707.

Fechete, I., Y. Wang, and J.C. Védrine, 2012, "The Past, Present and Future of Heterogeneous Catalysis", *Catalysis Today*, Vol. 189, pp. 2-27.

Ferencz, Zs., K. Baán, A. Oszkó, Z. Kónya, T. Kecskés, and A. Erdőhelyia, 2014, "Dry Reforming of CH_4 on Rh Doped Co/Al_2O_3 Catalysts", *Catalysis Today*, Vol. 228, pp. 123-130.

Filippi, C., X. Gonze, and C. J. Umrigar, 1996, "Generalized Gradient Approximations to Density Functional Theory: Comparison with Exact Results", *Recent Developments and Applications of Density Functional Theory*, *ed. J.M. Seminario*.

Frusteri, F., F. Arena, G. Calogero, T. Torre, and A. Parmaliana, 2001, "Potassium-enhanced Stability of Ni/MgO Catalysts in the Dry Reforming of Methane", *Catalysis Communications*, Vol. 1, pp. 49-56.

García-Diéguez, M., E. Finocchio, M. Á. Larrubia, L. J. Alemany, and G. Busca, 2010, "Characterization of Alumina-supported Pt, Ni and PtNi Alloy Catalysts for the Dry Reforming of Methane", *Journal of Catalysis*, Vol. 274, pp. 11-20.

Gökaliler, F., 2012, Characterization and Performance Analysis of Fuel Flexible OSR-WGS Catalysts, Ph.D. Thesis, Boğaziçi University.

Hehre, W. J., 2003, *A Guide to Molecular Mechanics and Quantum Chemical Calculations*, Wavefunction Inc., Irvine, CA, USA.

Huang, T., W. Huang, J. Huang, and P. Ji, 2011, "Methane Reforming Reaction with Carbon Dioxide over SBA-15 Supported Ni-Mo Bimetallic Catalysts", *Fuel Processing Technology*, Vol. 92, pp. 1868-1875.

Huang, W., L. Sun, P. Han, and J. Zhao, 2012, "CH_4 Dissociation on Co(0001): A Density Functional Theory Study", *Journal of Natural Gas Chemistry*, Vol. 21, pp. 98-103.

Jóźwiak, W. K., M. Nowosielska, and J. Rynkowski, 2005, "Reforming of Methane with Carbon Dioxide over Supported Bimetallic Catalysts Containing Ni and Noble Metal I. Characterization and Activity of SiO_2 Supported Ni-Rh Catalysts", *Applied Catalysis A: General,* Vol. 280, pp. 233-244.

Li, J., E. Croiset, and L. Ricardez-Sandoval, 2012, "Methane Dissociation on Ni (100), Ni (111), and Ni (553): A Comparative Density Functional Theory Study", *Journal of Molecular Catalysis A: Chemical*, Vol. 365, pp. 103-114.

Li, K., Z. Zhou, Y. Wang, and Z. Wu, 2013, "A Theoretical Study of CH_4 Dissociation on NiPd(111) Surface", *Surface Science*, Vol. 612, pp. 63-68.

Liu, H., R. Zhang, R. Yan, J. Li, B. Wang, and K. Xie, 2012, "Insight into CH_4 Dissociation on NiCu Catalyst: A First-Principles Study", *Applied Surface Science*, Vol. 258, pp. 8177-8184.

Liu, H., B. Wang, M. Fan, N. Henson, Y. Zhang, B. F. Towler, H. G. Harris, 2013, "Study on Carbon Deposition Associated with Catalytic CH_4 Reforming by Using Density Functional Theory", *Fuel,* Vol. 113, pp.712-718.

Liu, H., R. Zhang, R. Yan, B. Wang, and K. Xie, 2011, "CH_4 dissociation on NiCo (111) surface: A first-principles study", *Applied Surface Science*, Vol. 257, No. 21, pp. 8955-8964.

Luisetto, I., S. Tuti, and E. D. Bartolomeo, 2012, "Co and Ni Supported on CeO_2 as Selective Bimetallic Catalyst for Dry Reforming of Methane", *International Journal of Hydrogen Energy*, Vol. 37, pp. 15992-15999.

Lunsford, J. H., 2000, "Catalytic Conversion of Methane to More Useful Chemicals and Fuels: A Challenge for the 21st Century", *Catalysis Today*, Vol. 63, pp. 165-174.

Ma, S-H., X-T. Zu, and Z-Y. Jiao, 2008, "CO Adsorption on Magnetic Co(0001) Surface: A Study of Density Functional Theory", *Solid State Communications*, Vol. 147, pp. 152-156.

Mark, M. F., F. Mark, and W. F. Maier, 1997, "Reaction Kinetics of the CO_2 Reforming of Methane", *Chemical Engineering Technology,* Vol. 20, pp. 361-370.

Materials Studio Data Sheet: $DMol^3$, 2011, Reprinted with permission of Accelrys Software Inc., Accelrys Sofware Inc., San Diego, USA, http://accelrys.com/products/datasheets/dmol3.pdf, [Accessed May 2014].

Materials Studio Overview, 2011, Reprinted with permission of Accelrys Software Inc., Accelrys Sofware Inc., San Diego, http://accelrys.com/products/datasheets/materials-studio-overview.pdf, [Accessed May 2014].

McGuire, N. E., N. P. Sullivan, O. Deutschmann, H. Zhu, and R. J. Kee, 2011, "Dry Reforming of Methane in A Stagnation-Flow Reactor Using Rh Supported on Strontium-substituted Hexaaluminate", *Applied Catalysis A: General*, Vol. 394, pp.

257-265.

Menegazzo, F., M. Signoretto, F. Pinna, P. Canton, and N. Pernicone, 2012, "Optimization of Bimetallic Dry Reforming Catalysts by Temperature Programmed Reaction", *Applied Catalysis A: General*, Vol. 439-440, pp. 80-87.

Meshkani, F., and M. Rezaei, 2011, "Ni Catalysts Supported on Nanocrystalline Magnesium Oxide for Syngas Production by CO_2 Reforming of CH_4", *Journal of Natural Gas Chemistry*, Vol. 20, pp. 198-203.

Miguel, S.R., I. M. J. Vilella, S.P. Maina, D. San José-Alonso, M. C. Román-Martínez, and M. J. Illán-Gómez, 2012, "Influence of Pt Addition to Ni Catalysts on the Catalytic Performance for Long Term Dry Reforming of Methane", *Applied Catalysis A: General*, Vol. 435-436, pp. 10-18.

Mihaylova, A., K. Hadjiivanov, S. Dzwigaj, and M. Che, 2006, "Remarkable Effect of the Preparation Technique on the State of Cobalt Ions in BEA Zeolites Evidenced by FTIR Spectroscopy of Adsorbed CO and NO, TPR and XRD", *Journal of Physical Chemistry B*, Vol. 110, pp. 19530-19536.

Ni, J., L. Chen, J. Lin, and S. Kawi, 2012, "Carbon Deposition on Borated Alumina Supported Nano-Sized Ni Catalysts for Dry Reforming of CH_4", *Nano Energy*, Vol. 1, 674-686.

Olsbye, U., T. Wurzel, and L. Mleczko, 1997, "Kinetic and Reaction Engineering Studies of Dry Reforming of Methane over a $Ni/La/Al_2O_3$ Catalyst", *Industrial & Engineering Chemistry Research*, Vol. 36, pp. 5180-5188.

Özkara-Aydınoğlu, Ş. and A.E. Aksoylu, 2011, "CO_2 reforming of methane over Pt-Ni/Al_2O_3 catalysts: Effects of catalyst composition, and water and oxygen addition to the feed", *International Journal of Hydrogen Energy,* Vol. 36, pp. 2950-2959.

Özkara-Aydınoğlu, Ş., A. E. Aksoylu, and E. Özensoy, 2009, "The Effect of Impregnation

Strategy on Methane Dry Reforming Activity of Ce Promoted Pt/ZrO_2, *International Journal of Hydrogen Energy*, Vol. 34, pp. 9711-9722.

Özkara-Aydınoğlu, Ş., and A. E. Aksoylu, 2010, "Carbon Dioxide Reforming of Methane Over Co-X/ZrO_2 Catalysts (X=La, Ce, Mn, Mg, K)", *Catalysis Communications*, Vol. 11, 1165-1170.

Pakhare, D., C. Shaw, D. Haynes, D. Shekhawat, and J. Spivey, 2013, "Effect of Reaction Temperature on Activity of Pt- and Ru-substituted Lanthanum Zirconate Pyrochlores ($La_2Zr_2O_7$) for Dry (CO_2) Reforming of Methane (DRM)", *Journal of CO_2 Utilization*, Vol. 1, pp. 37-42.

Payne, M. C., M. P. Teter, D. C. Allan, T. A. Arias, and J. D. Joannopoulos, 1992, "Iterative Minimization Techniques fır ab initio Total-energy Calculations: Molecular Dynamics and Conjugate Gradients", *Review of Modern Physics*, Vol. 64, No.4, pp. 1045-1097.

Pompeo, F., N. N. Nichio, M. M. V. M. Souza, D. V. Cesar, O. A. Ferretti, and M. Schmal, 2007, "Study of Ni and Pt Catalysts Supported on α-Al_2O_3 and ZrO_2 Applied in Methane Reforming with CO_2", *Applied Catalysis A: General,* Vol. 316, pp. 175-183.

Qi, Q., X. Wang, L. Chen, and B. Li, 2013, "Methane Dissociation on Pt(111), Ir(111) and PtIr(111) Surface: A Density Functional Theory Study", *Applied Surface Science*, Vol. 284, pp. 784-791.

Rostrup-Nielsen, J. R. and J-H. Bak Hansen, 1993, "CO_2- Reforming of Methane over Transition Metals", *Journal of Catalysis*, Vol. 144, pp. 38-49.

Rostrup-Nielsen, J. R., 2004, "Fuels and Energy for the Future: The Role of Catalysis", *Catalysis Reviews: Science and Engineering*, Vol. 46, No. 3-4, pp. 247-270.

Ruckenstein, E., and H. Y. Wang, 2002, "Carbon Deposition and Catalytic Deactivation

during CO_2 Reforming of CH_4 over Co/γ-Al_2O_3 Catalysts", *Journal of Catalysis*, Vol. 205, pp. 289-293.

San José-Alonso, D., J. Juan-Juan, M. J. Illán-Gómez, and M. C. Román-Martínez, 2009, "Ni, Co and Bimetallic Ni-Co Catalysts for the Dry Reforming of Methane", *Applied Catalysis A: General*, Vol. 371, pp. 54-59.

San José-Alonso, D., M. J. Illán-Gómez, and M. C. Román-Martínez, 2011, "K and Sr Promoted Co Alumina Supported Catalysts for the CO_2 Reforming of Methane", *Catalysis Today*, Vol. 176, pp. 187-190.

Selen, B., 2003, *Production of Hydrogen from Light Hydrocarbons via Indirect Partial Oxidation on Bimetallic Catalysts*, M.S. Thesis, Boğaziçi University.

Sholl, D. S. and J. A. Steckel, 2009, *Density Functional Theory*, John Wiley & Sons, Inc., New Jersey, USA.

Song, D., J. Li, and Q. Cai, 2007, "In Situ Diffuse Reflectance FTIR Study of CO Adsorbed on a Cobalt Catalyst Supported by Silica with Different Pore Sizes", *Journal of Physical Chemistry C*, Vol. 111, pp. 18970-18979.

Stagg-Williams, S. M., F. B. Noronha, G. Fendley, and D. E. Resasco, 2000, "CO_2 Reforming of CH_4 over Pt/ZrO_2 Catalysts Promoted with La and Ce Oxides", *Journal of Catalysis*, Vol. 194, pp. 240-249.

Ulla, M.A., R. Spretz, E. Lombardo, W. Daniell, and H. Knözinger, 2001, "Catalytic combustion of methane on Co/MgO: characterisation of active cobalt sites", *Applied Catalysis B:Environmental,* Vol. 29, pp. 217-229.

Valderrama, G., C. U. de Navarro, and M. R. Goldwasser, 2013, "CO_2 reforming of CH_4 over Co-La-based perovskite-type catalyst precursors", *Journal of Power Sources*, Vol. 234, pp. 31-37.

Wang T., M. D. Porosoff, and J. G. Chen, 2014, "Effects of Oxide Supports on the Water-gas Shift Reaction over Pt-Ni Bimetallic Catalysts: Activity and Methanation Inhibition", *Catalysis Today*, Vol. 233, pp. 61-69.

Wang, S., and G.Q.M. Lu, 1999, "A Comprehensive Study on Carbon Dioxide Reforming of Methane over Ni/γ-Al_2O_3", *Industrial & Engineering Chemistry Research*, Vol. 38, pp. 2615-2625.

Wang, S-G., D-B. Cao, Y-W. Li, J. Wang, and H. Jiao, 2005, "CO_2 Dissociation on Ni Surfaces", *Journal of Physical Chemistry B*, Vol. 109, pp. 18956-18963.

Wang, S-G., D-B. Cao, Y-W. Li, J. Wang, and H. Jiao, 2006, CH_4 Dissociation on Ni Surfaces: Density Functional Theory Study, *Surface Science,* Vol. 600, pp. 3226-3234.

Wang, Z., X-M. Cao, J. Zhu, and P. Hu, 2014, "Activity and Coke Formation of Nickel and Nickel Carbide in Dry Reforming: A Deactivation Scheme from Density Functional Theory", *Journal of Catalysis*, Vol.311, pp. 469-480.

Watwe, R. M., H. S. Bengaard, J. R. Rostrup-Nielsen, J. A. Dumesic, and J. K. Nørskov, 2000, "Theoretical Studies of Stability and Reactivity of CH_x Species on Ni(111)", *Journal of Catalysis*, Vol. 189, pp. 16-30.

Xu, J., W. Zhou, Z. Lid, J. Wang, and J. Ma, 2009, "Biogas Reforming for Hydrogen Production over Nickel and Cobalt Bimetallic Catalysts", *International Journal of Hydrogen Energy*, Vol. 34, pp. 6646-6654.

Xu, L., Y. Liu, Y. Li, Z. Lin, X. Ma, Y. Zhang, M. D. Argyle, and M. Fan, 2014, "Catalytic CH_4 Reforming with CO_2 over Activated Carbon Based Catalysts", *Applied Catalysis A: General,* Vol. 469, pp. 387-397.

Yates, J. T., and J. K. Johnson, 2007, *Molecular Physical Chemistry for Engineers*, University Science Books, USA.

Yu, X., N. Wang, W. Chu, and M. Liu, 2012, "Carbon Dioxide Reforming of Methane for Syngas Production over La-Promoted NiMgAl Catalysts Derived from Hydrotalcites", *Chemical Engineering Journal*, Vol. 209, pp. 623-632.

Yung, M. M., Z. Zhao, M. P. Woods, U. S. Ozkan, 2008, "Preferential Oxidation of Carbon Monoxide on CoO_x/ZrO_2", *Journal of Molecular Catalysis A: Chemical*, Vol. 279, pp. 1-9.

Zeng, S., L. Zhang, X. Zhang, Y. Wang, H. Pan, and H. Su, 2012, "Modification Effect of Natural Mixed Rare Earths on $Co/\gamma\text{-}Al_2O_3$ Catalysts for CH_4/CO_2 Reforming to Synthesis Gas", *International Journal of Hydrogen Energy*, Vol. 37, pp. 9994-10001.

Zhang, Z.L and X.E. Verykios, 1994, "Carbon Dioxide Reforming of Methane to Synthesis Gas over Supported Ni", *Catalysis Today*, Vol. 21, pp. 589-595.

Zhu, Y-A., D. Chen, X-G. Zhou, and W-K. Yuan, 2009, "DFT Studies of Dry Reforming of Methane on Ni Catalyst", *Catalysis Today*, Vol.148, pp. 260-267.

Zuo, Z., W. Huang, P. Han, and Z. Li, 2010, "A Density Functional Theory Study of CH_4 Dehydrogenation on Co(111)", *Applied Surface Science*, Vol. 256, pp. 5929-5934.